

1 Scalable nonparametric clustering with unified marker gene 2 selection for single-cell RNA-seq data

3

4 Chibuikem Nwizu^{1,2}, Madeline Hughes³, Michelle L. Ramseier⁴⁻⁸, Andrew W. Navia⁴, Alex K. Shalek⁴⁻⁸,
5 Nicolo Fusi³, Srivatsan Raghavan^{4,9-11,§}, Peter S. Winter^{4,§}, Ava P. Amini^{3,§,†}, and Lorin Crawford^{3,§,†}

6 **1 Center for Computational Molecular Biology, Brown University, Providence, RI, USA**

7 **2 Warren Alpert Medical School of Brown University, Providence, RI, USA**

8 **3 Microsoft Research, Cambridge, MA, USA**

9 **4 Broad Institute of MIT and Harvard, Cambridge, MA, USA**

10 **5 Institute for Medical Engineering and Science, Massachusetts Institute of Technology,
11 Cambridge, MA, USA**

12 **6 Koch Institute for Integrative Cancer Research, Massachusetts Institute of Technology,
13 Cambridge, MA, USA**

14 **7 Department of Chemistry, Massachusetts Institute of Technology, Cambridge, MA, USA**

15 **8 Ragon Institute of MGH, MIT, and Harvard, Cambridge, MA, USA**

16 **9 Department of Medical Oncology, Dana-Farber Cancer Institute, Boston, MA, USA**

17 **10 Harvard Medical School, Boston, MA, USA**

18 **11 Department of Medicine, Brigham and Women's Hospital, Boston, MA, USA**

19 **§ Authors Contributed Equally**

20 **† Corresponding E-mail: ava.amini@microsoft.com; lcrawford@microsoft.com**

21 Abstract

22 Clustering is commonly used in single-cell RNA-sequencing (scRNA-seq) pipelines to characterize cellular
23 heterogeneity. However, current methods face two main limitations. First, they require user-specified
24 heuristics which add time and complexity to bioinformatic workflows; second, they rely on post-selective
25 differential expression analyses to identify marker genes driving cluster differences, which has been shown
26 to be subject to inflated false discovery rates. We address these challenges by introducing nonparamet-
27 ric clustering of single-cell populations (NCLUSION): an infinite mixture model that leverages Bayesian

28 sparse priors to identify marker genes while simultaneously performing clustering on single-cell expression
29 data. NCLUSION uses a scalable variational inference algorithm to perform these analyses on datasets
30 with up to millions of cells. Through simulations and analyses of publicly available scRNA-seq studies,
31 we demonstrate that NCLUSION (i) matches the performance of other state-of-the-art clustering tech-
32 niques with significantly reduced runtime and (ii) provides statistically robust and biologically relevant
33 transcriptomic signatures for each of the clusters it identifies. Overall, NCLUSION represents a reli-
34 able hypothesis-generating tool for understanding patterns of expression variation present in single-cell
35 populations.

36 **Introduction**

37 Recent advances in sequencing technologies have increased the throughput of genomic studies to millions
38 of single cells, necessitating computational workflows to explore and analyze these data¹. In single-cell
39 RNA sequencing (scRNA-seq), unsupervised clustering and marker gene selection are integral steps in
40 the exploratory phase of analyses^{2–5}. Clustering facilitates the identification of cell types, while marker
41 gene selection enables the annotation of gene modules and cluster-specific biological programs. However,
42 there has yet to be a consensus on the best approach to clustering cells and identifying the transcriptomic
43 signatures that characterize them^{6,7}. This has resulted in a multitude of proposed clustering methods for
44 single-cell data, many of which are reliant on various user-defined heuristics that prevent practitioners
45 from performing an unbiased survey of data and limit each method’s “out-of-the-box” applicability when
46 analyzing multiple studies.

47 Many current clustering approaches take a subset of highly variable genes as input, use dimensionality
48 reduction techniques to simplify the representation of single-cell expression for these genes, and then
49 perform clustering on top of this reduced representation. K-nearest neighbor (KNN) algorithms⁸, for
50 example, generate nearest-neighbor (NN) graphs using transcriptomic similarity scores between cells
51 and then perform Louvain clustering on the estimated graphs. Popular methods such as Seurat⁹ and
52 scLCA¹⁰ use principal component analysis (PCA) and singular value decomposition to learn a lower-
53 dimensional representation of cells, respectively. Ensemble approaches such as scCCESS-SIMLR¹¹ learn
54 over a mixture of kernels to generate a final cell-cell similarity matrix which is then used in a spectral
55 clustering algorithm.

56 Notably, selecting an appropriate embedding for single-cell data is not always a straightforward task.
57 Previous studies have shown that if the generated lower-dimensional representation does not accurately
58 capture underlying biological relationships between cells, then both the quality of clustering and the
59 generalizability of findings in downstream analyses can be compromised^{12,13}. Factors such as the number
60 of highly variable genes retained during data preprocessing and the number of components used to define
61 the lower-dimensional embedding can affect the ability of a clustering algorithm to identify fine-grained
62 differences between cell types^{7,14}. Furthermore, nearly all state-of-the-art clustering methods require
63 users to specify the number of clusters K to be used in the algorithm. Strategies such as consensus-
64 finding^{11,15}, outlier detection¹⁶, and iterative cluster merging and splitting^{17–19} rely on human-in-the-
65 loop interactive steps within their algorithms to determine an “optimal” choice for K . Generally, requiring
66 users to make these additional decisions can add significant time and complexity when using clustering
67 as a preliminary analysis in bioinformatic workflows.

68 Perhaps the biggest limitation of current single-cell clustering algorithms is that most do not directly
69 identify top marker genes that are driving the inference of different biologically significant clusters; in-
70 stead, they use post-selective inference to find genes that are differentially expressed between the inferred
71 cell groups^{7,20}. Since the point of clustering algorithms is to separate dissimilar data into different groups,
72 it is expected *a priori* that there are differences between the groups and any test statistics computed by
73 comparing the groups are likely to be inflated due to “data double dipping”. Many studies have shown
74 that performing this post-selective inference uncorrected can lead to inflated type I error rates^{20,21}.
75 Though there has been work developed to correct for post-selection, these are still in nascent, and most
76 do not yet scale to high-dimensional settings^{22–27}. Recently, others have proposed unified frameworks
77 for simultaneous clustering and marker gene selection using hierarchical tree-based algorithms²⁸, regular-
78 ized copula models²⁹, and *post hoc* sensitivity measures³⁰. However, these approaches rely on arbitrary
79 thresholding to find “significant” marker genes and fail to theoretically test a well-defined null hypothesis,
80 making them difficult to biologically interpret.

81 We present “Nonparametric CLustering of SIngle-cell populatiONs” (NCLUSION): a unified Bayesian
82 nonparametric framework that simultaneously performs clustering and marker gene selection. NCLU-
83 SION works directly on normalized single-cell count data, bypassing the need to perform dimensionality
84 reduction. By modeling the expression of each gene as a sparse hierarchical Dirichlet process normal mix-
85 ture model^{31–37}, NCLUSION both learns the optimal number of clusters based on the variation observed

86 between cellular expression profiles and uses sparse prior distributions to identify genes that significantly
87 influence cluster definitions. The key to our proposed integrative framework is that clustering and ex-
88 tracting marker genes concurrently is a more efficient approach to the exploratory analysis of scRNA-seq
89 data, as it effectively allows each process to inform the other. Most importantly, our approach eliminates
90 the need for human-in-the-loop decisions, significantly reducing the runtime and complexity of these
91 analyses. Altogether, NCLUSION mitigates the need for heuristic choices (e.g., choosing specific lower-
92 dimensional embeddings), avoids iterative hyper-parameter optimization, bridges the interpretability gap
93 suffered by many unsupervised learning algorithms in single-cell applications, and scales to accommodate
94 the growing sizes of emerging scRNA-seq datasets.

95 **Results**

96 **NCLUSION simplifies traditional clustering workflows**

97 Conventional scRNA-seq clustering approaches include numerous steps that require user heuristics or
98 human-in-the-loop decisions which increase runtime and complexity (Fig 1A). These can range from
99 deciding how to optimally embed high-dimensional expression data into a lower-dimensional space to
100 selecting the number of clusters, K , to identify in the data. Furthermore, current methods require that
101 marker gene selection is performed post-clustering, which can lead to inflated rates of false discovery^{20,21}.
102 In this work, we aim to address these challenges using a new approach: NCLUSION.

103 NCLUSION leverages a Bayesian nonparametric mixture modeling framework to reduce the number
104 of choices that users need to make while simultaneously performing variable selection to identify top
105 cluster-specific marker genes for downstream analyses (Fig 1B; see Methods for details). There are three
106 key components of our model formulation that distinguish it from traditional bioinformatic workflows.
107 First, NCLUSION is fit directly on single-cell expression matrices and does not require the data to be
108 embedded within a lower-dimensional space. Second, we implicitly assume *a priori* that cells can belong
109 to one of infinitely many different clusters. This is captured by placing a Dirichlet process prior over the
110 cluster assignment probabilities for each cell. By allowing the number of possible clusters $K = \infty$, we
111 remove the need for users to iterate through different values until they find the optimal choice. Third,
112 NCLUSION assumes that not all genes are important when assigning cells to a given cluster. To model
113 this, we place a spike and slab prior on the mean expression of each gene within each cluster. This prior

114 shrinks the mean of genes that play an insignificant role in cluster formation towards zero.

115 To identify cluster-specific marker genes, we start by estimating posterior inclusion probabilities
116 (PIPs), which represent our confidence that a gene's mean expression within a cluster is nonzero. These
117 PIPs act as a signature that can be used to distinguish clusters. Since NCLUSION fits each gene and
118 cell independently, signatures learned between clusters can share the same subsets of genes. To select for
119 unique cell type markers, we multiply each PIP with a usage weight, which is calculated by performing
120 min-max normalization over the proportion of clusters in which a gene is determined to be statistically
121 significant (i.e., using the median probability model threshold³⁸ $PIP \geq 0.5$). We use these adjusted in-
122 clusion probabilities with the effect size sign (ESS) and strictly standardized mean difference (SSMD) of
123 each gene to filter for significant genes that are substantially up-regulated (indicated by positive ESS and
124 large SSMD values). The genes remaining after filtering make up cluster-specific marker gene modules
125 that provide insight into the biological features underlying cluster assignments.

126 To enable efficient posterior inference that can scale as the size of scRNA-seq datasets continues to
127 grow, we train NCLUSION using variational expectation-maximization (EM). This algorithm leverages a
128 “mean-field” assumption to approximate the true posterior distribution over model parameter estimates
129 with a product of simpler distributions^{39–41}. In training, our objective is to minimize the Kullback–Leibler
130 (KL) divergence between the variational posterior and the true posterior⁴². Optimization during model
131 fitting occurs using a coordinate ascent procedure where parameters are sequentially updated based on
132 their gradients (Methods and Supplementary Material). With this variational approach, NCLUSION is
133 capable of scaling well up to 1 million cells without applying any dimensionality reduction to the input
134 data.

135 We evaluated the runtime of NCLUSION against a set of state-of-the-art single-cell clustering methods
136 using publicly available datasets. The methods we used for comparison include: Seurat⁹, scLCA¹⁰, K-
137 nearest neighbors followed by the Leiden clustering algorithm (KNN+Leiden)⁴³, SOUP⁴⁴, and scCCESS-
138 SIMLR¹¹. Each of these methods operates by first reducing the dimensionality of the input data and
139 then performing clustering on the reduced representation. To the best of our knowledge, NCLUSION is
140 the only method to date that clusters on the expression matrix directly while jointly identifying cluster-
141 specific salient genes. NCLUSION does not incur additional runtime cost due to this model design choice.
142 In fact, NCLUSION boasts a faster runtime compared to other methods, particularly as the number of
143 cells in a dataset grows. We showcase this scalability on the BRAIN-LARGE⁴⁵ dataset (Fig 1C). To

144 facilitate comparison across all baseline methods, we follow Lopez et al.¹⁴ and limit the analysis to
145 720 genes, while subsampling the number of cells from 500 to 1 million cells. As a practical reference,
146 we use a grey dotted line to highlight the runtime for each method at the median scRNA-seq dataset
147 size as determined in 2020: 31,000 cells⁴⁶. We observed that only NCLUSION and KNN+Leiden were
148 able to scale past 100,000 cells, while NCLUSION was the only method able to run on 1 million cells.
149 Additionally, NCLUSION records competitive runtimes across varying numbers of genes (Fig S1). These
150 scalability results show the potential of NCLUSION’s utility for emerging large-scale single-cell studies.

151 NCLUSION accurately identifies clusters and marker genes in simulations

152 We used simulations to evaluate the performance of NCLUSION in controlled settings. Here, we used
153 `scDesign3`⁴⁷ to generate synthetic datasets consisting of 10,000 cells and 1,000 genes (due to computa-
154 tional constraints of the software) distributed over five clusters. We considered four different scenarios
155 (with 20 replicates per scenario), where we varied cluster size and marker gene composition (Methods).
156 Scenario I was the simplest, where we evenly distributed all cells across the five clusters, and each cluster
157 had 50 marker genes. In Scenarios II and III, all five clusters had 50 marker genes, but one cluster had
158 significantly fewer cells than the other four clusters. Lastly, in Scenario IV, each of the five clusters had
159 the same number of cells, but one cluster had a signature of only 20 marker genes, while the other four
160 clusters had 50 marker genes each.

161 We first compared the cluster identification accuracy of NCLUSION with the previously described al-
162 gorithms: Seurat⁹, scLCA¹⁰, K-nearest neighbors followed by the Leiden clustering algorithm (KNN+Leiden)⁴³,
163 SOUP⁴⁴, and scCCESS-SIMLR¹¹. The relatively smaller size of these simulated datasets also allowed
164 us to include three additional widely used methods: CIDR⁴⁸, SC3⁴⁹, and scDeepCluster⁵⁰. We should
165 highlight that all competing methods, except for NCLUSION, first perform dimensionality reduction
166 prior to clustering, allowing us to evaluate the impact of dimensionality reduction on cluster recovery.

167 The normalized mutual information (NMI) and adjusted Rand index (ARI) were calculated to quan-
168 titatively evaluate the clustering results given by each algorithm. In all scenarios, scDeepCluster had
169 the best performance, with NCLUSION, scLCA, and scCCESS-SIMLR rounding out the top four. The
170 reason for scDeepCluster’s top performance is that it first performs Leiden clustering on principal com-
171 ponents from the expression data to obtain the initial cluster assignments. Then, it uses a deep neural
172 network to refine the cluster assignments; therefore, performance is highly dependent on the initialization

173 of the cluster assignments and on the success of the initial clustering. NCLUSION, on the other hand,
174 only performs clustering once to achieve comparable results. Notably, all methods performed relatively
175 worse in Scenarios II and III than their performance in Scenarios I and IV (Fig S2; Table S1) due to the
176 class imbalance in how the cells were distributed across clusters.

177 We also evaluated the performance of NCLUSION on marker gene detection using the same simulated
178 datasets and compared it with three popular differential expression algorithms: DUBStepR⁵¹, singleCell-
179 Haystack²⁵, and FESTEM⁵². Notably, of these methods, only NCLUSION is able to find cluster-specific
180 marker genes. FESTEM uses an alternative algorithm (via the Scott-Knott test) to assign marker genes
181 to clusters found by an independent clustering method, while both DUBStepR and singleCellHaystack
182 aim to identify differentially expressed genes. To that end, we evaluated the global marker gene detec-
183 tion of each model using true positive rate (TPR), false discovery rate (FDR), and false positive rate
184 (FPR; computed as 1-Specificity for each method). We found no statistically significant differences when
185 comparing the median power of NCLUSION to the other approaches (Kruskal-Wallis *H*-test $P > 0.99$;
186 Fig S3 and Table S2). However, importantly, NCLUSION and FESTEM were the only two methods to
187 have high power while maintaining a low FDR and FPR. On the other hand, singleCellHaystack and
188 DUBStepR achieved similar power but only because they incorrectly labeled many genes as being marker
189 genes (resulting in markedly higher FDR and FPR).

190 **NCLUSION achieves competitive clustering performance on PBMC data with 191 less runtime**

192 Next, we assessed the quality of clustering done by NCLUSION as compared to other baseline approaches
193 on real data. Here, we analyzed scRNA-seq from FACS-purified peripheral blood mononuclear cells
194 (PBMCs)⁵³. This dataset captures 10 cellular populations, including CD14+ monocytes, CD34+ cells,
195 major lymphoid lineages (B and T cells), as well as other phenotypic lineages within the T cell population,
196 including CD4+ helper T cells, CD8+ cytotoxic T cells, CD4+ regulatory T cells, and CD4+ memory T
197 cells. After quality control (Methods), the final dataset contained 94,615 cells and 5,000 genes with the
198 highest standard deviation (post log-normalization)^{20,54}. We evaluated the performance of NCLUSION,
199 Seurat, scLCA, the KNN+Leiden algorithm, SOUP, and scCCESS-SIMLR by comparing inferred cluster
200 assignments to the cell type annotations from the original study, which were obtained via a combination
201 of FACS analysis and clustering with Seurat⁵³ (Fig 3A-B).

202 To qualitatively assess clustering performance, we used contingency heat maps to evaluate how well
203 each method captured the unique cell types across clusters (Fig 3C). For a given method, each n -th row
204 of the heat map represents an annotation from the original study and each k -th column represents an
205 inferred cluster identified by the method. The color saturation of each (n, k) -th element in the heat map
206 indicates the fraction of a n -th cell annotation that a given method assigned to the k -th inferred cluster.
207 Overall, all baselines were able to distinguish the B cell population from other cells, and each approach
208 uniquely clustered a majority of the CD14+ monocytes together (Fig 3C). Furthermore, all methods
209 except scCCESS-SIMLR and KNN+Leiden were able to separate the natural killer (NK) cell population
210 with an inferred cluster occupancy rate of greater than 90% (Table S3). NCLUSION's performance was
211 most similar to that of Seurat (χ^2 -test $P = 0.99$ when assessing independence between their contingency
212 tables). Both methods were able to identify major PBMC cell lineages and were the only approaches to
213 divide the B cell, cytotoxic CD8+ T cells, and regulatory T cells into subpopulations⁵⁵ (Fig 3C).

214 As a quantitative assessment of each method's clustering performance, we used the FACS-derived
215 experimental annotations as reference labels and computed NMI and ARI, each measuring how well the
216 clustering algorithm's labels matched the reference labels (Methods). For both metrics, values closer to
217 1 indicate better clustering performance. To assess the robustness and consistency of each method, we
218 ran them on five different randomly subsampled partitions containing 80% of the cells in the dataset. We
219 report the mean metric score for each clustering algorithm across these partitions, along with correspond-
220 ing 95% confidence intervals (Fig 3D). NCLUSION outperformed all competing approaches across both
221 metrics. It obtained the highest mean NMI coefficient of 0.80 ($\pm 1.62 \times 10^{-2}$ standard deviation), with
222 Seurat and scLCA each scoring lower values of 0.77 ($\pm 2.78 \times 10^{-3}$) and 0.62 ($\pm 3.04 \times 10^{-2}$), respectively.
223 These differences were statistically significant, as determined by two-sided t-tests ($P = 1.08 \times 10^{-3}$ and
224 $P = 1.90 \times 10^{-6}$, respectively). When comparing performance using the ARI, NCLUSION remained
225 competitive and significantly outperformed other methods (Table S4). Specifically, NCLUSION achieved
226 a higher mean ARI of 0.67 ($\pm 2.02 \times 10^{-2}$) when compared to 0.62 ($\pm 2.48 \times 10^{-3}$; two-sided t-tests
227 $P = 1.17 \times 10^{-3}$) for Seurat and 0.50 ($\pm 2.52 \times 10^{-2}$; two-sided t-tests $P = 3.10 \times 10^{-6}$) for scLCA,
228 respectively.

229 Lastly, NCLUSION recorded the shortest runtime for this analysis without any iterative processes
230 or optimization of hyperparameters. It finished approximately 254 seconds (4.23 minutes) faster than
231 Seurat, more than 12,900 seconds (215.00 mins or 3.58 hrs) faster than scLCA, and more than 41,331

232 seconds (688.85 mins or 11.48 hrs) faster than scCCESS-SIMLR.

233 NCLUSION is well-powered to identify PBMC-specific marker genes

234 The key distinguishing property of NCLUSION is its inherent ability to perform variable selection. NCLU-
235 SION thus provides users with cluster labels for each cell as well as unique gene signatures that define
236 each cluster. The statistical model underlying NCLUSION selects cluster-specific marker genes based on
237 two criteria: (i) an adjusted posterior inclusion probability, $\text{PIP}(j; k)$, which provides evidence that the
238 j -th gene's mean expression is uniquely nonzero within the k -th cluster, (ii) the sign of the j -th gene's
239 effect, $\text{ESS}(j; k)$, which is used to determine whether it is uniquely up-regulated or down-regulated within
240 the k -th cluster, and (iii) the magnitude of the j -th gene's effect, $\text{SSMD}(j; k)$, on the definition of the
241 k -th cluster (Methods). We assessed the marker genes identified by NCLUSION for each of the inferred
242 clusters in the PBMC dataset to determine whether they provide insights into the biology of different
243 cell types (Fig 4A-B).

244 Overall, NCLUSION successfully identified cluster-specific marker genes that are known to be associ-
245 ated with examined cell types (Fig 4C and Table S5). For example, in cluster 8 which has cells mapping
246 back to the cytotoxic and naive cytotoxic T cell population, we observed that NCLUSION correctly iden-
247 tified marker genes known to play an important role in cytotoxic T cell biology, such as *CD8A* (adjusted
248 $\text{PIP} = 0.90$), *CD8B* (adjusted $\text{PIP} = 0.70$)⁵⁶, and *CD27* (adjusted $\text{PIP} = 0.62$)⁵⁷. Furthermore, genes
249 associated with cytotoxicity, such as *GZMM*, tended to be selected in clusters largely containing CD8+ T
250 cells (Cluster 8; adjusted $\text{PIP} = 0.60$) and NK cells (Cluster 2; adjusted $\text{PIP} = 0.61$)—two cell types that
251 have been shown to have functionally similar cytotoxic activity⁵⁸. In other clusters, where we observed
252 genes associated with both B cells (e.g., in Cluster 1, *CD19*, adjusted $\text{PIP} = 1.00$; *LINC00926*, adjusted
253 $\text{PIP} = 1.00$; *MS4A1*, $\text{PIP} = 0.90$)⁵⁹⁻⁶¹ and myeloid lineages (e.g., in Cluster 3, *MS4A6A*, $\text{PIP} = 1.00$;
254 *S100A8*, adjusted $\text{PIP} = 0.93$; *LYZ*, $\text{PIP} = 0.90$)⁶², NCLUSION distinguished genes known to play an
255 important role in T cell biology as statistically significant. This observation suggests that NCLUSION
256 accounted for the variance among T cell and T cell-like expression patterns when distinguishing cell types
257 in the PBMC dataset. We observed that our criteria for cluster-specific marker genes, based on high PIPs
258 and positive ESS scores, strongly agreed with the relative over-expression of each gene in its respective
259 cluster (Fig 4C). Imposing a threshold on SSMD allowed NCLUSION to filter out less relevant genes,
260 narrowing the list of cluster-specific over-expressed genes to those most salient.

261 To further evaluate marker gene quality, we computed gene module scores in order to compare the
262 normalized expression for signature genes across clusters (Fig 4D and Table S6). Here, we find that each
263 module exhibits the highest expression within its respective cluster, with the most definitive signatures
264 occurring within the B (inferred cluster 1), NK (inferred cluster 2), monocytic (inferred cluster 3),
265 and CD34+ cells (inferred cluster 4) (Fig 4E and Fig S4). In clusters that contained heterogeneous
266 combinations of T cell subpopulations, we still see an increased relative expression among cluster-specific
267 marker genes, although not as distinct as in the other cell types.

268 As an additional analysis, we compared the similarity between the marker genes identified by NCLU-
269 SION with the list of marker genes that are identified by using a *post hoc* differential expression analysis
270 with Seurat. Here, we took the FACS-derived experimental annotations from Zheng et al.⁵³ and found
271 differentially expressed genes by doing a one-versus-all Wilcoxon rank sum test for each cluster (mirroring
272 the typical procedure in a conventional bioinformatic workflow). As expected, this post-selective infer-
273 ence procedure resulted in Seurat identifying a multitude of candidate marker genes for each cell type,
274 even after Bonferroni correction. A direct comparison between NCLUSION and Seurat showed that the
275 proposed Bayesian variable selection approach in the NCLUSION framework results in smaller and more
276 refined transcriptomic signatures for downstream investigation (Fig 4F and Figs S5- S6). For example,
277 NCLUSION identified 134 cluster-specific marker genes for NK cells, 97% of which were also included
278 in the 1,780 marker genes selected *post hoc* by Seurat. In total, an average of 96% of the marker genes
279 identified by NCLUSION were included in the much larger sets of differentially expressed genes selected
280 by Seurat across each of the FACS-annotated cell types.

281 Over-representation analysis using gene product annotations in Gene Ontology (GO) further confirmed
282 that the selective set of gene modules inferred by NCLUSION reflect known immune cell biology⁶³⁻⁶⁵
283 (Fig 4G-H and Table S7). For example, in the cluster containing predominantly B cells (inferred cluster
284 1), we observed an up-regulation of B cell receptor signaling (adjusted $P = 6.68 \times 10^{-7}$), B cell activation
285 (adjusted $P = 2.3 \times 10^{-7}$), and B cell proliferation (adjusted $P = 2.51 \times 10^{-7}$)^{66,67}. Notably, some of
286 the biologically relevant GO terms found when using NCLUSION were not statistically significant when
287 applying the larger sets of marker genes provided *post hoc* by Seurat. For instance, in the cluster with
288 NK cells (inferred cluster 2), significant gene sets from NCLUSION included the positive regulation of
289 leukocyte chemotaxis (adjusted $P = 1.53 \times 10^{-4}$) and positive regulation of natural killer cell chemotaxis
290 (adjusted $P = 4.88 \times 10^{-6}$)⁶⁸⁻⁷⁰. We also observed enrichment of the up-regulation of natural killer cell

291 mediated cytotoxicity (adjusted $P = 3.81 \times 10^{-5}$), consistent with the known highly cytotoxic behavior
292 of NK cells^{68,71}. Each of these gene sets was insignificant when using differentially expressed genes
293 from Seurat (Fig 4G). Lastly, in the monocyte-dominated cluster (inferred cluster 3), the NCLUSION-
294 generated module was enriched for macrophage activation involved in immune response (adjusted P
295 = 2.41×10^{-5}) and antigen-presenting activity (e.g., MHC Class II antigen presentation, adjusted P =
296 5.39×10^{-4}). Complete marker gene and GO analyses for all clusters inferred by NCLUSION and Seurat
297 as a baseline in the PBMC dataset can be found in Table S7. Together, these results demonstrate that
298 NCLUSION can identify cluster-specific gene signatures that reflect underlying cellular phenotypes.

299 NCLUSION's performance generalizes to the other single-cell datasets

300 Finally, we assessed the generalizability of NCLUSION by testing it on three additional large scRNA-seq
301 datasets of various sample sizes: a pancreatic ductal adenocarcinoma (PDAC) dataset from Raghavan
302 et al.⁷² with $N = 23,042$ cells; an acute myeloid leukemia (AML) dataset from van Galen et al.⁷³ with
303 $N = 43,690$ cells; and a tissue immune (IMMUNE) atlas dataset from Domínguez Conde et al.⁷⁴ with
304 $N = 88,057$ cells. These datasets represent a range of tissue and disease states to assess our method's
305 performance in different use cases. Both the PDAC and AML datasets contain a mixture of malignant
306 and non-malignant cells from different patient biopsies, while the IMMUNE dataset contains healthy
307 white blood cells from different anatomical locations. After performing quality control (Methods), we
308 had a total of 5,000 genes with the highest standard deviation (after log-normalization) for the analysis.

309 We observed similar scalability in the runtime of NCLUSION and competing baselines on all three
310 datasets (Fig 5A). NCLUSION maintains its computational efficiency, now only being slightly outper-
311 formed by Seurat on the PDAC and AML datasets due to longer convergence time in its variational
312 EM algorithm. We also found that NCLUSION continued to remain competitive in terms of clustering
313 performance. When quantitatively evaluating the clustering ability of NCLUSION versus the competing
314 baselines using the annotations provided by the original studies, NCLUSION was often statistically sig-
315 nificantly better (as determined via a two-sided t-test, $P < 0.05$) according to ARI and NMI across all
316 datasets (Fig 5B-C, Figs S7-S19, and Table S4).

317 We then analyzed the interpretability of the cluster-specific marker genes inferred by NCLUSION
318 (Fig 5D-G, Figs S8-S24, and Tables S8-S19). For brevity, we highlight just notable results from the
319 PDAC and IMMUNE datasets in the main text. Additional analyses for the AML dataset can be found

320 in the Supplementary Material (see Figs S12-S17 and Tables S16-S19).

321 To begin, we focused on evaluating the gene modules generated from the NCLUSION inferred clusters
322 in the PDAC dataset (Fig 5D-G). As with the PBMC data, we observed higher module expression within
323 the respective clusters (Fig 5F). NCLUSION appeared to use immune cell signatures as the primary axis
324 for distinguishing malignant and non-malignant populations (Fig 5E and Table S10). For example, the
325 inferred cluster 6 predominantly contained cells that were originally annotated as NK and T cells by
326 Raghavan et al.⁷². This inferred cluster had immune cell type specific marker genes such as *CD2* (PIP =
327 0.92), *GZMB* (PIP = 0.85), *IL7R* (PIP = 0.85), and *NCAM1* (PIP = 1.00)^{75,76} (Fig 5D). An additional
328 GO analysis of this cluster showed an enrichment of natural killer cell mediated cytotoxicity (adjusted *P*
329 = 6.60×10^{-9}) and T cell receptor signaling (adjusted *P* = 1.17×10^{-21}) (Fig 5G).

330 Notably, the other clusters that primarily contained non-malignant cells (inferred clusters 4, 5, 11,
331 12, 13, and 14) also directly aligned with cell type labels originally annotated by Raghavan et al.⁷². For
332 the clusters that primarily contained malignant and metastatic cells (i.e., inferred clusters 1, 2, 3, 9, and
333 10), a GO analysis revealed an enrichment of extracellular matrix (ECM) organization and cell migration
334 processes (Fig 5G). Importantly, however, NCLUSION also had the power to divide these cells into more
335 granular subpopulations based on their level of differentiation. For example, the inferred cluster 9 was
336 enriched for both cell migration processes (e.g., MET-activated PTK2 signaling, adjusted *P* = 2.97×10^{-5} ;
337 MET-promoted cell motility, adjusted *P* = 4.02×10^{-5}) and fibroblast cell activity (pancreatic fibroblasts,
338 adjusted *P* = 2.1×10^{-9} ; collagen formation, adjusted *P* = 1.13×10^{-7})^{77,78}.

339 Finally, we evaluated the granularity of NCLUSION's clustering on the IMMUNE dataset, which
340 contained 33 manually annotated labels from experts⁷⁴. When analyzing this study, NCLUSION was
341 able to delineate between multiple T cell sub-lineages, whereas methods like Seurat, KNN+Leiden, and
342 scCCESS SIMLR merged these subpopulations into 1 or 2 clusters. For example, the inferred cluster 12
343 by NCLLUSION was enriched ($\sim 95\%$ occupancy rate) for CD8+ effector memory (T_{EM}) and effector
344 memory cells re-expressing CD45RA (T_{EMRA}), while NCLUSION's inferred cluster 8 was enriched ($\sim 90\%$
345 occupancy rate) for CD8+ tissue-resident memory (T_{RM}). These two populations have been shown to
346 be functionally distinct subpopulations in the CD8+ T cell lineage^{79,80}. Likewise NCLUSION's inferred
347 clusters 6 and 10 were enriched ($\sim 77\%$ and $\sim 72\%$ occupancy rates, respectively) for functionally distinct
348 subpopulations of CD4+ T cells, namely T follicular helper cells (Tfh) and CD4+ effector/effectector memory
349 T cells, respectively^{79,81,82} (Table S12).

350 The GO analysis of NCLUSION-generated gene modules also showed an enrichment of T cell pheno-
351 types. The inferred cluster 12's top ontology term was indeed “CD8+ Effector Memory T4” (adjusted
352 $P = 4.18 \times 10^{-9}$), while the inferred cluster 10 had “CD4+ Central Memory T1” as a top enriched term
353 (adjusted $P = 3.53 \times 10^{-3}$). Similar results showing how NCLUSION-generated gene modules granularly
354 distinguish these cellular populations can be found in the Supplementary Material (Table S15).

355 Discussion

356 We present NCLUSION: a scalable Bayesian nonparametric framework designed to serve as an unbiased
357 method for inferring phenotypic clusters and identifying cluster-specific marker genes in scRNA-seq ex-
358 periments. We show how our approach simplifies traditional single-cell transcriptomic workflows, which
359 often rely on the transformation of the data to a lower-dimensional representation to facilitate clustering
360 and iteratively tune the number of clusters used to obtain optimal results. In contrast, NCLUSION
361 operates on the full normalized gene expression matrix, eliminating the need for transformation to a
362 lower-dimensional space; infers the optimal number of clusters without iterative user refinement; and
363 simultaneously identifies the cluster-specific marker genes that significantly drive the clustering. By
364 leveraging a variational inference algorithm, NCLUSION can scale to scRNA-seq studies with a million
365 cells. Through the analysis of a collection of large-scale publicly available datasets, we show that NCLU-
366 SION not only achieves clustering performance comparable to state-of-the-art methods but also provides
367 refined sets of gene candidates for downstream analyses. By unifying clustering and marker gene selec-
368 tion, NCLUSION provides a flexible and unified statistical framework for inferring complex differential
369 gene expression patterns observed in heterogeneous tissue populations^{21,83,84}.

370 The current implementation of the NCLUSION framework offers many directions for future devel-
371 opment and applications. First, NCLUSION assumes a normal mixture model for log-normalized gene
372 expression data. We use this assumption both because log-based transformations have been shown to
373 reduce the effects of sparsity in single-cell analyses^{20,85} and because the Gaussian-based specification of-
374 fers computational advantages for scalable posterior inference. Still, future extensions of the NCLUSION
375 framework should explore the utility of Poisson- and negative binomial-based likelihoods to deal with the
376 zero-inflated nature of scRNA-seq studies in their raw form.

377 Second, the current formulation of NCLUSION models the gene expression of each cell indepen-

378 dently and does not consider, for example, the correlation between genes with similar functionality or
379 co-expression patterns between genes within the same signaling pathway. One possible extension of
380 NCLUSION would be to incorporate additional genomic information into the sparse prior distributions
381 used for Bayesian variable selection. For example, previous studies have proposed an integrative approach
382 where the importance of a variable also depends on an additional set of covariates^{40,86,87}. In the case of
383 single-cell applications, we could assume that the prior probability of the j -th gene being a marker of the
384 k -th cluster is also dependent upon its cellular pathway membership. Unlike the current spike-and-slab
385 prior NCLUSION implements, this new prior would assume that biologically related pathways contain
386 shared marker genes, essentially integrating the concept of gene set enrichment analysis into cluster-
387 ing. An alternative approach would be to extend NCLUSION to incorporate non-diagonal correlation
388 structures by exploring sparse covariance models, which could provide a balance between the need for
389 maintaining computational efficiency while representing a richer set of gene dependencies^{88,89}.

390 Third, although it helps NCLUSION scale to large datasets, variational expectation-maximization
391 (EM) algorithms are known to both produce slightly miscalibrated parameter estimates and underes-
392 timate the total variation present within a dataset^{41,90,91}. While this does not greatly affect the per-
393 formance of NCLUSION in the evaluations presented in this paper, this can be seen as a limitation
394 depending on the application of interest. For example, in the PBMC dataset, NCLUSION is unable to
395 resolve all the different T cell subtypes that were annotated by Zheng et al.⁵³ (Fig 3). This is most likely
396 due to variational approximations being well-suited to describe the global variation across cells but at
397 the cost of smoothing over local variation between smaller subpopulations. Considering other (equally
398 scalable) ways to carry out approximate Bayesian inference may be relevant for future work⁹².

399 Lastly, a thrust of recent work in genomics has been to develop methods that identify spatially variable
400 marker genes as a key step during analyses of spatially-resolved transcriptomics data⁹³. Future efforts
401 could extend NCLUSION to this emerging modality by, for example, reformulating the method as a
402 spatial Dirichlet process mixture model⁹⁴.

403 In sum, NCLUSION provides a unified framework for simultaneous clustering and marker gene selec-
404 tion in single-cell transcriptomic data, yielding improvements in computational efficiency, interpretability,
405 and scalability. We envision that NCLUSION will accelerate key analytic steps universal to single-cell
406 analysis across diverse applications.

407 Materials and methods

408 Overview of NCLUSION

409 We provide a brief overview of the probabilistic framework underlying the “Nonparametric CLUstering
410 of SIngle-cell populatiONs” (NCLUSION) model. Detailed derivations of the algorithm are provided in
411 the Supplementary Material. Consider a study with single-cell RNA sequencing (scRNA-seq) expression
412 data for $n = 1, \dots, N$ cells that each have measurements for $j = 1, \dots, J$ genes. Let this dataset be
413 represented by the $N \times J$ matrix \mathbf{X} where the row-vector $\mathbf{x}_n = (x_{n1}, \dots, x_{nJ})$ denotes the expression
414 profile for the n -th cell. We assume that the log-normalized gene expression for each cell follows a sparse
415 hierarchical Dirichlet process normal mixture model^{31–33} of the form

$$416 \quad x_{nj} \sim \sum_{k=1}^{\infty} \pi_k \mathcal{N}(\nu_j + \mu_{jk}, \sigma_j^2) \quad (1)$$

417 where π_k represents the marginal (unconditional) probability that a cell belongs to the k -th cluster, ν_j
418 and σ_j^2 are the global means and variances for the j -th gene across all cells (i.e., not conditioned on
419 cluster identity), and μ_{jk} is the mean shift of expression for the j -th gene within the k -th cluster. There
420 are two key features in the model formulation of NCLUSION specified above. First, we assume that the
421 formation of clusters is driven by a few important genes that have mean expression shifted away from a
422 baseline gene-specific expression level, ν_j . To that end, we place a sparsity-inducing spike and slab prior
423 distribution on the mean effect of each gene

$$424 \quad \mu_{jk} \sim \eta \mathcal{N}(0, \lambda_{jk} \sigma_j^2) + (1 - \eta) \delta_0, \quad (2)$$

425 where δ_0 is a point mass at zero, λ_{jk} scales the global variance to form a cluster-specific “slab” distribution
426 for each gene, and η is the prior probability that any given gene has a nonzero effect when assigning a cell
427 to any cluster. In practice, there are many different ways to estimate η . Following previous work^{40,41,95–97},
428 one choice would be to assume a uniform prior over $\log \eta$ to reflect our lack of knowledge about the correct
429 number of “marker” genes for each cell type that is present in the data. Instead, in this work, we assume
430 $\eta \sim \text{Beta}(1, 1)$ to represent this uncertainty and learn its value during model inference. To facilitate
431 posterior computation and interpretable inference, we introduce a binary indicator variable $\rho_{jk} \in \{0, 1\}$

432 where we implicitly assume *a priori* that $\Pr[\rho_{jk} = 1] = \eta$. Alternatively, we say that ρ_{jk} takes on a
 433 value of 1 when the effect of a gene μ_{jk} on cluster assignment is nonzero and deviates from the baseline
 434 gene expression level ν_j . As NCLUSION is trained, the posterior mean for unimportant genes will trend
 435 towards the global mean (i.e., $\mu_{jk} \rightarrow 0$) as the model attempts to identify subsets of marker genes that
 436 are relevant for each cluster. We then use posterior inclusion probabilities (PIPs) as general summaries
 437 of evidence that the j -th gene is statistically important in determining when a cell is assigned to the k -th
 438 cluster where

$$439 \quad \text{PIP}(j; k) \equiv \Pr[\mu_{jk} \neq 0 \mid \mathbf{X}]. \quad (3)$$

440 The second key feature in Eq. (1) is that we do not assume to know the true number of clusters K .
 441 Instead, we take a nonparametric approach and attempt to learn K directly from the data. Once again,
 442 to facilitate posterior computation, we introduce a categorical latent variable ψ_n which indicates that the
 443 n -th cell is in the k -th cluster with prior probability π_k . Explicitly, we write this as $\Pr[\psi_n = k] = \pi_k$.
 444 Here, we implement the stick-breaking construction of the Dirichlet process³¹ where we say

$$445 \quad \boldsymbol{\pi} \sim \text{Dir}(\alpha_0 \boldsymbol{\beta}), \quad \beta_k \sim \chi_k \prod_{l=1}^{k-1} (1 - \chi_l), \quad \chi_k \sim \text{Beta}(1, \gamma_0) \quad (4)$$

446 with $\boldsymbol{\pi} = (\pi_1, \dots, \pi_{>K})$ having mean $\boldsymbol{\beta}$ and variance determined by the concentration hyper-parameters
 447 α_0 and γ_0 ⁹⁸. The concentration hyper-parameters α_0 and γ_0 are both non-negative scalars that effectively
 448 help to determine the number of clusters used in the model^{31,39}. Larger values for these parameters
 449 increase the model's sensitivity to variation in the data and encourage the creation of a greater number
 450 of smaller clusters. Smaller values for these parameters, on the other hand, decrease the model's sensitivity
 451 to variation in the data and encourage the creation of fewer larger clusters. In this work, we encourage the
 452 creation of fewer clusters and fix α_0 and γ_0 to be less than or equal to 1 (Supplementary Material). After
 453 model training, we use the posterior distribution over the latent categorical indicators $\Pr[\psi_n = k \mid \mathbf{X}]$ to
 454 determine the cluster assignment for each cell. It is worth noting that, although the prior number of
 455 normal components is infinite in Eq. (1), the posterior number of components after model fitting will
 456 be finite. This truncation reflects the fact that not all infinite states are used when conditioning on
 457 finite data⁹⁸. Additionally, the algorithm used to estimate the parameters in the NCLUSION software

458 penalizes empty clusters (see Supplementary Material), and, as a result, the model has the flexibility to
459 automatically adjust its complexity based on the inferred complexity of the data being analyzed. This
460 helps to increase the utility and adaptability of NCLUSION across a wide range of single-cell applications.

461 Selection of cluster-specific marker genes

462 NCLUSION jointly performs clustering on single-cell populations while also learning cluster-specific gene
463 signatures. To achieve this, we use the spike and slab prior distribution specified in Eq. (2) and the
464 resulting PIPs defined in Eq. (3) to find the most salient genes per cluster. Since the model fits to
465 each j -th gene expression for the n -th cell independently, signatures learned between clusters can share
466 subsets of the same genes. Genes that are identified as “important” across many different clusters can
467 effectively be seen as ubiquitous housekeeping variables rather than significant marker genes of unique
468 cell types. Therefore, we down-weight the inclusion probabilities to proportionally penalize genes based
469 on the number of clusters in which they appear

$$470 \quad \text{PIP}^*(j; k) = w_j \times \text{PIP}(j; k), \quad w_j = \left(1 - \frac{S_j}{K^*}\right) \bigg/ \left(1 - \frac{1}{K^*}\right) \quad (5)$$

471 where $K^* \leq K$ is the finite number of occupied clusters learned by the model, and S_j is the number of
472 clusters that the j -th gene is significant in according to a given selection threshold. We set this threshold
473 to be 0.5 which corresponds to the median probability criterion in Bayesian statistics³⁸.

474 While Eqs. (3) and (5) can be used to identify the genes that are differentially expressed in a given
475 cluster, they do not indicate the direction or magnitude of this shift. Therefore, for each gene, we combine
476 the adjusted posterior inclusion probabilities with effect size sign (ESS) and strictly standardized mean
477 difference (SSMD) measures to find the most salient markers per cluster. Here, we obtain the effect size
478 sign by taking the sign of Cohen’s d ⁹⁹ between the expression of the j -th gene for cells in the k -th cluster
479 and cells not in the k -th cluster (denoted by k')

$$480 \quad \text{ESS}(j; k) = \text{sgn} \left(\frac{\rho_{jk}\mu_{jk} - \bar{m}_{jk}}{\sigma_j} \right) \quad (6)$$

481 where, in addition to previous notation, $\bar{m}_{jk'} = \sum_{k'} \rho_{jk'} \mu_{jk'}/(K^* - 1)$ is the average mean shift for the
482 j -th gene in all clusters outside of the k -th. Here, $\text{sgn}(\cdot)$ is the piecewise sign function where $\text{sgn}(u) = +$

483 (i.e., positive) when $u > 0$, $\text{sgn}(u) = -$ (i.e., negative) when $u < 0$, and $\text{sgn}(u) = 0$ when $u = 0$.

484 The strictly standardized mean difference (SSMD) is a metric often used in high-throughput screenings
485 to test for the significance of an effect size magnitude^{100–103}. It is computed as the following

$$486 \quad \text{SSMD}(j; k) = \frac{\mu_{jk} - \bar{\mu}_{jk'}}{\sqrt{\sigma_j^2 [(N_k - 1)/N_k + (N_{k'} - 1)/N_{k'}]}} \quad (7)$$

487 where $\bar{\mu}_{jk'} = \sum_{k'} \mu_{jk'}/(K^* - 1)$ is the average global mean for the j -th gene in all clusters outside of the
488 k -th. Asymptotically, the SSMD follows a normal distribution^{100,101,103}. To determine a significant value,
489 we follow a previous procedure¹⁰³ by calculating a threshold $|\text{SSMD}(j; k)| \geq S^*(j; k)$ which controls for
490 a predetermined false positive rate (FPR). Here, this threshold is given by

$$491 \quad S^*(j; k) = \text{SSMD}_{min} + \Phi^{-1} \left(1 - \frac{\text{FPR}}{2} \right) \varsigma_{jk} \quad (8)$$

492 where FPR is set to 0.05, $\Phi^{-1}(\cdot)$ is the inverse cumulative distribution function of a standard normal,
493 and SSMD_{min} is the minimum SSMD magnitude that one considers to be significant. In practice, this
494 minimum value is often set between 0 and 0.25 in order to identify weak effect sizes. In the main text, we
495 follow previous work^{103–105} and let $\text{SSMD}_{min} = 0.15$. The parameter ς_{jk} is used to denote the asymptotic
496 variance which is given by

$$497 \quad \varsigma_{jk} = \frac{(N_k - 1)/N_k^2 + (N_{k'} - 1)/N_{k'}^2}{(N_k - 1)/N_k + (N_{k'} - 1)/N_{k'}} + \frac{(N_k - 1)^2/N_k^2 + (N_{k'} - 1)^2/N_{k'}^2}{2\sigma_j^2 [(N_k - 1)/N_k + (N_{k'} - 1)/N_{k'}]^3} (\mu_{jk} - \bar{\mu}_{jk'})^2. \quad (9)$$

498 In the main text, cluster-specific marker genes are selected as those that have a significant adjusted inclu-
499 sion probability and are notably up-regulated in a given cluster meaning that they satisfy the following
500 criteria: (1) $\text{PIP}^*(j; k) \geq 0.5$, (2) $\text{ESS}(j; k) = +$, and (3) $\text{SSMD}(j; k) \geq S^*(j; k)$, respectively.

501 Posterior inference via variational EM algorithm

502 We combine the likelihood in Eq. (1) and the prior distributions in Eqs. (2) and (4) to perform Bayesian
503 inference. In current scRNA-seq datasets, it is less feasible to implement traditional Markov Chain
504 Monte Carlo (MCMC) algorithms due to the large number of cells being studied. For model fitting, we
505 instead use a variational expectation-maximization (EM) algorithm^{31,32,98}, which allows us to estimate

506 parameters within an optimization framework. The overall goal of variational inference is to approximate
507 the true posterior distribution for model parameters using a set of approximating distributions. The
508 EM algorithm optimizes parameters such that it minimizes the Kullback-Leibler divergence between the
509 exact and approximate posterior distributions. To compute the variational approximations, we make the
510 mean-field assumption that the true posterior can be “fully-factorized”¹⁰⁶. The algorithm then follows two
511 general steps. In the first step, we iterate through a combination of hyper-parameter values and compute
512 variational updates for the other parameters using coordinate ascent. In the second step, we empirically
513 compute (approximate) posterior values for the main model parameters $\{\mu, \rho, \psi\}$. Detailed steps in the
514 variational EM algorithm, explicit coordinate ascent updates for the model parameters, pseudocode, and
515 other derivations are given in the Supplementary Material. Parameters in the variational EM algorithm
516 are initialized by taking random draws from their assumed prior distributions. Iterations in the algorithm
517 are terminated when at least one of two stopping criteria are met: (i) the difference between the lower
518 bound of two consecutive updates is within some small range (specified by argument ϵ), or (ii) a maximum
519 number of iterations is reached. For the analyses run in this paper, we set $\epsilon = 1$ for the first criterion
520 and used a maximum of 1×10^4 iterations for the second.

521 Simulation study design

522 **Generating simulated datasets.** To evaluate the robustness and sensitivity of NCLUSION under
523 controlled conditions, we generated synthetic single-cell RNA-seq datasets using `scDesign3`⁴⁷ (v.1.4.0).
524 The reference dataset we used was derived from the FACS-sorted peripheral blood mononuclear cell
525 (PBMC) dataset produced by Zheng et al.⁵³. Initial preprocessing for this reference dataset included
526 mitochondrial gene content assessment, ribosomal and hemoglobin gene filtering, and quality control to
527 remove both low-quality cells and lowly expressed genes. Highly variable genes (HVGs) were identified
528 using the `modelGeneVar` function in the `scran` R package, and the top 1000 HVGs were retained for
529 downstream simulation. We used five immune cell types (B cells, CD14+ monocytes, CD56+ natural
530 killer (NK) cells, cytotoxic T cells, and regulatory T cells) for these analyses. To ensure balanced
531 representation across cell types, we implemented a stratified subsampling scheme which selected an equal
532 number of cells per type while enforcing non-zero gene expression across all selected cells and genes.

533 Each simulated dataset comprised of $N = 10,000$ cells across five clusters and 1,000 genes where we
534 preserved realistic transcriptomic correlation structures through Gaussian copula modeling. Simulations

535 were conducted across four different scenarios (with 20 replicates per scenario), each varying in cluster
536 size imbalance and marker gene composition.

- 537 • **Scenario I:** Balanced clusters of 2000 cells per cell type, each with 50 marker genes.
- 538 • **Scenario II:** Imbalanced cluster design where one small cluster had 200 cells and the other four
539 larger clusters each had 2450 cells. All clusters contained 50 marker genes.
- 540 • **Scenario III:** Imbalanced cluster design where one cluster had 20 (rare) cells and the other four
541 larger clusters each had 2495 cells each. All clusters contained 50 marker genes.
- 542 • **Scenario IV:** Balanced clusters of 2000 cells per cell type, but one cluster had only 20 marker
543 genes while the other four clusters had 50 marker genes.

544 More specifically, synthetic datasets were generated using the `construct_data`, `fit_marginal`, `fit_copula`,
545 `extract_para`, and `simu_new` functions within `scDesign3` to create gene expression vectors using a neg-
546 ative binomial distribution that is conditioned on cell type from the reference data. To introduce differ-
547 entially expressed genes (DEGs), we first ranked genes by their cell type specific mean expression in the
548 reference data and sampled a number of top-ranked genes to be markers. Then in the synthetic data,
549 these DEGs were then artificially upregulated in one cluster while maintaining the baseline expression in
550 others. This was done by apply a log-fold change factor sampled uniformly over the interval [1.5, 2.5].
551 This ensured that we maintained realistic variance but still had distinct signal between cell types.

552 Real datasets and preprocessing

553 Below we briefly describe all of the datasets and the preprocessing steps used in this work. Each of these
554 datasets is relatively large (containing at least 20,000 cells) with unique molecular identifiers (UMI).
555 The latter is important because prior research suggests that UMIs provide enough information to avoid
556 overcounting issues due to amplification and zero-inflation^{14,107,108}. We use an asterisk by the BRAIN-
557 LARGE dataset to indicate that it was exclusively to test the scalability of NCLUSION and competing
558 methods; therefore, clustering performance was not recorded. For the other datasets, we use cell type
559 annotations provided by the original study as “true” reference labels during our analyses. Cells were
560 filtered for quality using a custom `scipy`¹⁰⁹ (v.1.9.1) pipeline script (see Software availability). Unless
561 otherwise stated, all data was preprocessed by taking the logarithm (to the base 2) of the counts, dividing

562 by a scaling factor of 10000, and then adding a pseudo-count of 1.0 for stability. Additionally, unless
563 otherwise stated, all results were produced using the top 5000 highly variable genes (HVG), which were
564 determined by sorting the standard deviation of the transformed counts³³.

565 **BRAIN-LARGE***. This dataset originally contains 1.3 million mouse brain cells from 10x Genomics⁴⁵.
566 During preprocessing, we subset the data to a collection of 720 genes following a procedure outlined by
567 Lopez et al.¹⁴. Next, we further filtered by only keeping cells that had at least one of these genes
568 expressed. This left a total of 64,071 cells. Since the original study did not provide cell labels, we exclu-
569 sively used this dataset to compare runtime performance. To do so, we up-sampled by randomly selecting
570 groups of 64,071 cells to create a synthetic dataset of 1 million cells. We report the runtime for each
571 method on datasets with 500, 1K, 5K, 10K, 50K, 100K, 500K, and 1M cells.

572 **PBMC**. We took scRNA-seq data from fluorescence-activated cell sorted (FACS) populations of pe-
573 ripheral blood mononuclear cells (PBMCs) provided by Zheng et al.⁵³ and concatenated each population
574 into one dataset. During preprocessing, we filtered out genes that were expressed in fewer than three
575 cells. We also dropped cells with (i) fewer than 200 genes expressed, (ii) greater than 20% mitochondrial
576 reads, and (iii) fewer than 5% ribosomal reads. This resulted in a final dataset with 94,615 high-quality
577 cells representing 10 distinct cell types.

578 **PDAC**. We used scRNA-seq data from pancreatic ductal adenocarcinoma (PDAC) tissue obtained
579 from 23 patients according to methods documented in Raghavan et al.⁷². This dataset contains 23,042
580 total cells made up of 15,302 non-malignant cells of 11 distinct cell types and 7,740 malignant cells.

581 **AML**. The scRNA-seq data obtained from van Galen et al.⁷³ contains 43,690 acute myeloid leukemia
582 (AML) and non-malignant donor cells taken from 16 AML patients, 5 healthy donors, and 2 cell lines. It
583 is comprised of 13,489 patient-derived malignant cells, 23,005 non-malignant donor cells, 6,018 cells from
584 the MUTZ-3 AML cell line, and 1,178 cells from the OCI-AML3 cell line. To account for the biological
585 differences between cell lines and donor cells of the same cell type annotation, we appended the cell line
586 name onto cell type labels where applicable, producing 33 distinct cell types overall. To process the data,
587 we filtered out all cells with “unclear” cell state labels, retaining only “malignant” or “non-malignant”
588 cells.

589 **IMMUNE.** We obtained filtered scRNA-seq data from approximately 330,000 immune cells from 12
590 organ donors in Domínguez Conde et al.⁷⁴. To mitigate batch effects, we isolated 88,057 cells that were
591 taken from a single organ donor (donor D496) with uniform chemistry annotations, containing 44 distinct
592 immune cell types.

593 Other methods

594 We selected five additional methods to compare against the performance of NCLUSION in real data
595 and in simulations: (1) a Louvain algorithm implemented using the `FindClusters` function in Seurat⁹
596 (v.4.3.0.1); (2) a spectral clustering method called scLCA¹⁰ (v.0.0.0.9000), which optimizes both intra-
597 and inter-cluster similarity; (3) a combination of a K-Nearest Neighbor (KNN) classifier with the Louvain
598 community detection algorithm to find clusters implemented via `scikit-learn`⁴³ (v.1.2.2) and `scenpy`¹⁰⁹
599 (v.1.9.1), respectively; (4) a semi-soft clustering algorithm called SOUP⁴⁴ (v.0.0.0.9000); and (5) an
600 ensemble method called scCCESS-SIMLR (v.0.2.1), which leverages the spectral clustering approach
601 SIMLR^{11,110}. In the simulation experiments, we also compared the clustering performance of NCLUSION
602 against three additional methods: (6) a consensus clustering method, SC3⁴⁹(v.1.34.0); (7) a deep-learning
603 based method, scDeepCluster⁵⁰ (v.1.0.0); and (8) an imputation and dimensionality reduction method,
604 CIDR⁴⁸ (v.0.1.5). Also in simulations, when assessing the ability of NCLUSION to perform robust marker
605 gene selection, we compare it against: (9) a method that leverage differential correlation patterns in the
606 local structure of a PCA-derived cell neighborhood graph, DUBStepR⁵¹ (v.1.2.0); (10) a feature selection
607 via an EM algorithm, FESTEM⁵² (v.1.2.1); and (11) a divergence-based strategy with permutation tests,
608 singleCellHaystack²⁵ (v.1.0.2). Additional details about each method are provided in the Supplementary
609 Material.

610 Evaluation metrics

611 Below we describe the metrics and approaches used to compare performance across all methods. Our
612 clustering evaluation procedure used extrinsic metrics that require reference labels to serve as the ground
613 truth in our calculations.

614 **Normalized mutual information (NMI).** This metric is a normalized variant of mutual information
615 (MI). It is an entropy-based metric that captures the amount of shared information between the inferred

616 label distribution and the reference label distribution. NMI ranges between [0, 1] where 1 represents total
 617 information sharing between label sets and 0 represents no information sharing between label sets. NMI
 618 is calculated by

$$619 \quad \text{NMI} = \frac{I(Q; R)}{\sqrt{\mathbb{H}(Q)\mathbb{H}(R)}}$$

620 where Q and R are the empirical label distributions from the inferred and reference labels, respectively.
 621 The function $I(\cdot)$ is the mutual information between the inferred labels distribution and reference labels
 622 distributions; $\mathbb{H}(\cdot)$ represents the Shannon entropy of a given label distribution^{110,111}.

623 **Adjusted Rand index (ARI).** This metric captures the similarity between labels inferred by a method
 624 and the reference labels. It is based on the Rand index (RI) but corrects for the measurement's sensitivity
 625 to chance. ARI ranges between [-1, 1] where 1 represents perfect agreement between label sets, 0 represents
 626 random agreement, and -1 represents perfect disagreement. ARI is calculated by

$$627 \quad \text{ARI} = \frac{\sum_{ij} \binom{n_{ij}}{2} - \left[\sum_i \binom{a_i}{2} \sum_j \binom{b_j}{2} \right] \binom{n}{2}}{1/2 \left[\sum_i \binom{a_i}{2} + \sum_j \binom{b_j}{2} \right] - \left[\sum_i \binom{a_i}{2} \sum_j \binom{b_j}{2} \right] \binom{n}{2}}$$

628 where n_{ij} , a_i , and b_j are values obtained from a contingency table, and $n = \sum_{ij} n_{ij}$ ¹¹⁰⁻¹¹².

629 **Metrics to evaluate marker gene selection in simulations.** In the simulation studies, we evaluated
 630 the accuracy of marker gene detection of NCLUSION and competing methods by treating the task as a
 631 classification problem. In order to do so, we defined the confusion matrix defined below.

		(Inferred Label)		Total
		Marker gene	Non-marker gene	
(True Label)	Marker gene	TP	FN	b_1
	Non-marker gene	FP	TN	b_2
Total		a_1	a_2	n

Table 1. Confusion matrix showing true and inferred marker gene labels.

632 Here, TP represents the number of correctly identified marker genes (true positives), FN represents the
 633 number of incorrectly identified marker genes (false negatives), TN represents the number of correctly
 634 identified non-marker genes (true negatives), and FP represents the number of incorrectly identified non-

635 marker genes (false positives). In the table above, we let a_1 and a_2 be the total number of genes inferred
636 as markers and the total number of genes not inferred as markers, respectively. Likewise, we let b_1 and
637 b_2 be the total number of genes that are truly markers and non-markers, respectively. It follows that
638 the total number of genes is defined as $n = a_1 + b_1 + a_2 + b_2$. From here, we can compute the following
639 metrics.

- 640 • **True positive rate (TPR; also referred to as power)** captures the proportion of correctly
641 identified marker genes using a given method. It is defined as $\text{TPR} = \text{TP}/(\text{TP}+\text{FP})$.
- 642 • **False discovery rate (FDR)** details the proportion of all identified marker genes that are actually
643 non-marker genes. It is defined as $\text{FDR} = \text{FP}/(\text{TP} + \text{FP})$.
- 644 • **False positive rate (FPR)** captures the proportion of non-marker genes that will be incorrectly
645 labeled marker genes. It is defined as $\text{FPR} = \text{FP}/(\text{TN} + \text{FP})$.

646 Note that the false positive rate can also be computed as $\text{FPR} = 1 - \text{Specificity}$.

647 **Normalized module expression.** Genes with significantly adjusted PIPs in Eq. (5), positive ESS
648 in Eq. (6), and significant SSMD in Eq. (7) were used to generate modules (i.e., a collection of marker
649 genes) for each cluster. We calculated a score for each cluster to assess the exclusivity of expression within
650 each module. This was done using the `score_genes` function in `scipy` (v.1.10.4). The violin plots were
651 generated using the `violinplot` function in `matplotlib` (v.3.10.0).

652 **Gene set over-enrichment analysis.** We also performed gene set enrichment analysis on each of
653 the learned gene modules across clusters. This was done via an over-enrichment analysis within the
654 `GSEapy` package¹¹³ (v.1.1.5) in Python (v.3.11.0). This method uses a hypergeometric test to calculate
655 the enrichment of genes in a supplied module with respect to the gene sets within an ontology. In
656 this work, we use the ontology labeled `GO_Biological_Process_2025`^{63–65,114}, `Tabula_Sapiens`^{115,116},
657 `Azimuth_Cell_Types_2021`¹¹⁷, `KEGG_2021_Human`^{118–120}, and `Reactome_2022`^{121–128}. The gene sets in
658 this particular ontology represent a combination of biological processes, pathways, and phenotypes. In
659 this analysis, we use q -values to determine the enrichment of a given gene set with a significance threshold
660 set to 0.05. The q -value is the analog of a p -value that has been corrected for testing multiple hypotheses
661 (i.e., an adjusted P).

662 Software availability

663 An open-source software implementation of NCLUSION is available on GitHub at <https://github.com>
664 [/microsoft/Nclusion.jl](https://github.com/microsoft/Nclusion.jl). Guided tutorials and all code needed to reproduce the results and figures in
665 this work can be found at <https://microsoft.github.io/Nclusion.jl/>.

666 Data availability

667 All of the datasets analyzed in this paper are publicly available. The PDAC dataset from Raghavan
668 et al.⁷² can be accessed at https://singlecell.broadinstitute.org/single_cell/study/SC
669 [P1644/microenvironment-drives-cell-state-plasticity-and-drug-response-in-pancrea](https://singlecell.broadinstitute.org/single_cell/study/SC)
670 [tic-cancer#/](https://singlecell.broadinstitute.org/single_cell/study/SC). The AML data from van Galen et al.⁷³ can be found at <https://www.dropbox.co>
671 [m/s/399x045zc57fiut/Seurat_AML.rds?dl=0](https://www.dropbox.co). The BRAIN-LARGE dataset can be accessed at
672 <https://www.10xgenomics.com/datasets/1-3-million-brain-cells-from-e-18-mice-2-s>
673 [standard-1-3-0](https://www.10xgenomics.com/datasets/1-3-million-brain-cells-from-e-18-mice-2-s). The individual PBMC data from Zheng et al.⁵³ can be downloaded directly from
674 <https://www.10xgenomics.com/resources/datasets>. Lastly, the immune cell atlas dataset can be
675 accessed at https://cellgeni.cog.sanger.ac.uk/pan-immune/CountAdded_PIP_global_object_f
676 [or_cellxgene.h5ad](https://cellgeni.cog.sanger.ac.uk/pan-immune/CountAdded_PIP_global_object_f).

677 Acknowledgements

678 We thank members of the Crawford, Raghavan, and Shalek Labs for insightful comments on earlier
679 versions of this manuscript. This research was conducted by using a combination of computational
680 resources and services provided by Microsoft Research and the Center for Computation and Visualization
681 at Brown University. This research was also supported in part by an Alfred P. Sloan Research Fellowship
682 and a David & Lucile Packard Fellowship for Science and Engineering awarded to LC. CN was a trainee
683 supported under the Brown University Predoctoral Training Program in Biological Data Science (NIH
684 T32GM128596). SR is supported by NCI K08 award 1K08CA260442, the Claudia Adams Barr Program
685 in Innovative Basic Cancer Research, and the Dana-Farber Cancer Institute Hale Family Center for
686 Pancreatic Cancer Research. Any opinions, findings, and conclusions or recommendations expressed in
687 this material are those of the author(s) and do not necessarily reflect the views of any of the funders.

688 **Author contributions**

689 CN, APA, and LC conceived the study and developed the methods. CN and MH developed the algorithm
690 and software. CN, MH, and MR led the analyses. SR, PSW, APA, and LC provided resources, supervised
691 the project, and conducted secondary analyses. All authors interpreted the results and wrote and revised
692 the manuscript.

693 **Declaration of interests**

694 SR holds equity in Amgen. PSW reports compensation for consulting/speaking from Engine Ventures
695 and AbbVie unrelated to this work. AKS reports compensation for consulting and/or scientific advisory
696 board membership from Honeycomb Biotechnologies, Cellarity, Ochre Bio, Relation Therapeutics, Fog
697 Pharma, Bio-Rad Laboratories, IntrECate Biotherapeutics, Passkey Therapeutics and Dahlia Biosciences
698 unrelated to this work. SR and PSW receive research funding from Microsoft. MH, NF, APA, and LC are
699 employees of Microsoft and own equity in Microsoft. All other authors have declared that no competing
700 interests exist.

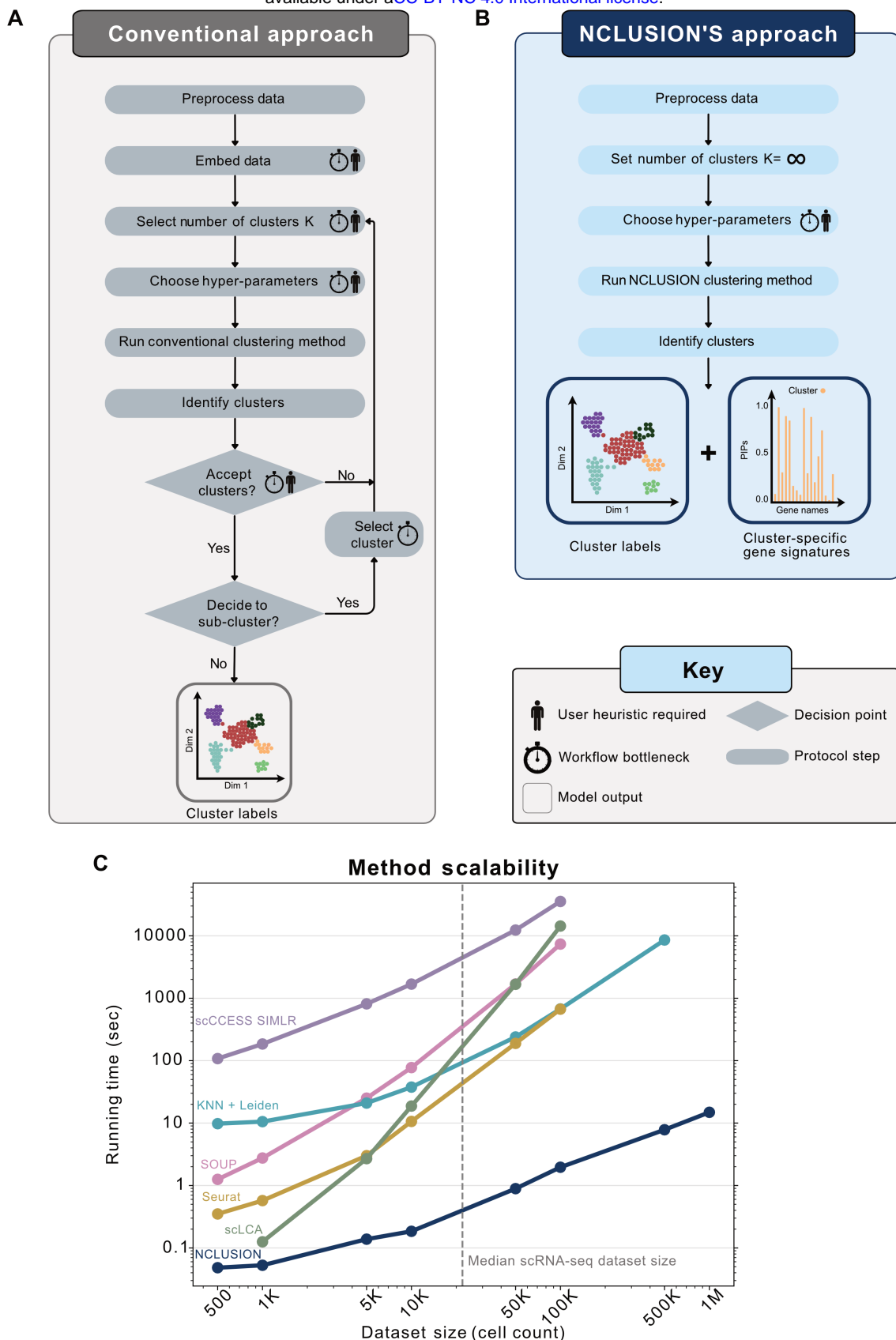


Fig 1. NCLUSION provides a scalable, unified workflow for both clustering and marker gene selection in single-cell analysis. (A) Conventional clustering algorithms require user heuristics and decision making steps that increase wall clock runtime (e.g., selection and human-in-the-loop refinement of the number of clusters K). **(B)** The nonparametric workflow of NCLUSION reduces the number of choices and heuristics that users have to make while also performing cluster-specific variable selection to identify top marker genes for downstream investigation. **(C)** Runtimes of NCLUSION and other baselines on the BRAIN-LARGE dataset with a fixed set of 720 genes and an increasing sample size ranging from $N = 500$ to 1 million cells.

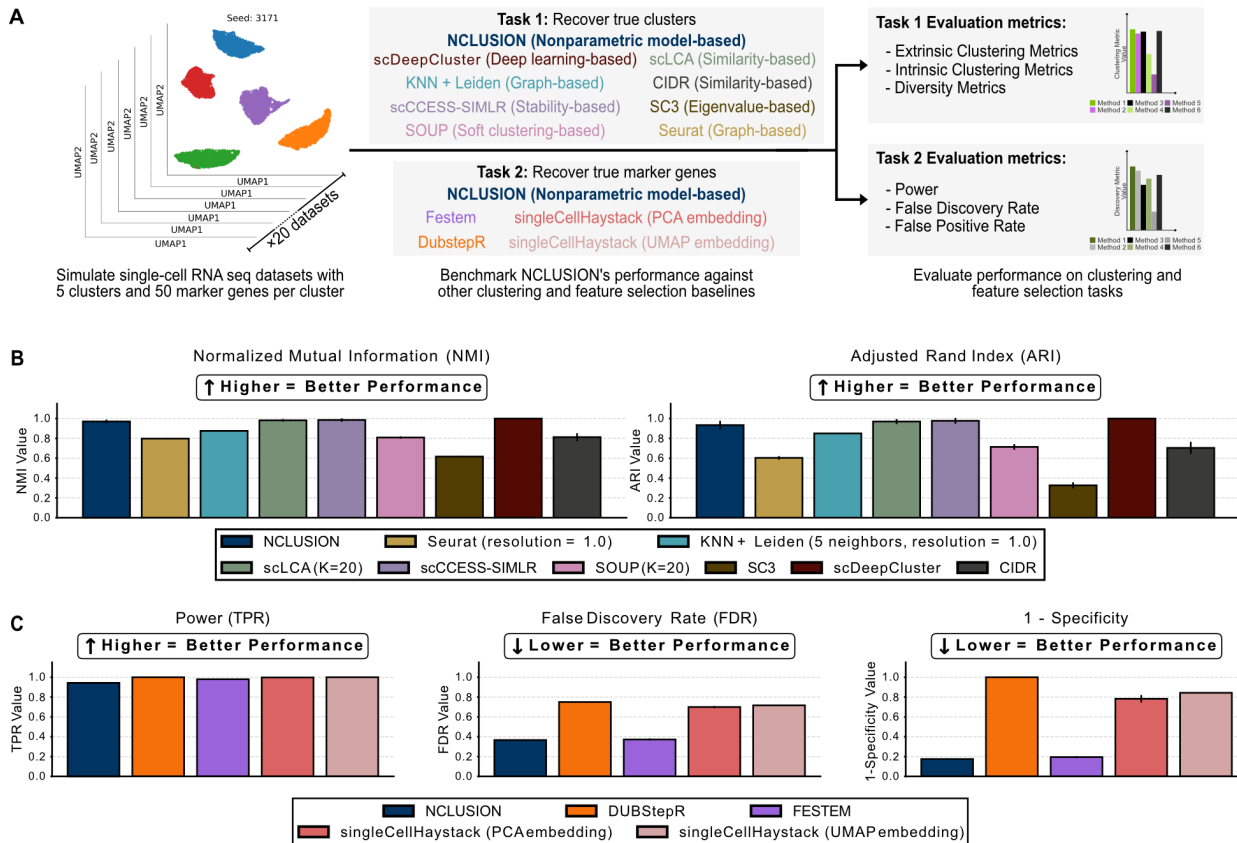


Fig 2. Comparing NCLUSION and competing algorithms on performing clustering and marker gene selection in a simulation study. Depicted are results for Scenario I where we evenly distributed all synthetically generated cells across five clusters and each cluster had a unique set of 50 marker genes. **(A)** Overview of the simulation framework used for evaluating the quality of clustering and marker gene selection for NCLUSION and each competing method. **(B)** Inferred cluster labels were compared to “true” annotations created during the simulation, where performance was measured according to (left) normalized mutual information (NMI) and (right) adjusted Rand index (ARI). **(C)** Assessment of marker gene selection was done on the global scale, where methods were evaluated on how well they could detect a “true” causal gene without taking cluster assignment into account. This was due to the limitation of competing methods not being able to identify cluster-specific genes. Evaluations were done by measuring the true positive rate (TPR; or power), false discovery rate (FDR), and false positive rate (FPR; computed as 1-Specificity) for each approach. Results for (B) and (C) are based on 20 simulations, with each bar plot representing the mean and the error bars covering a $\pm 95\%$ confidence interval.

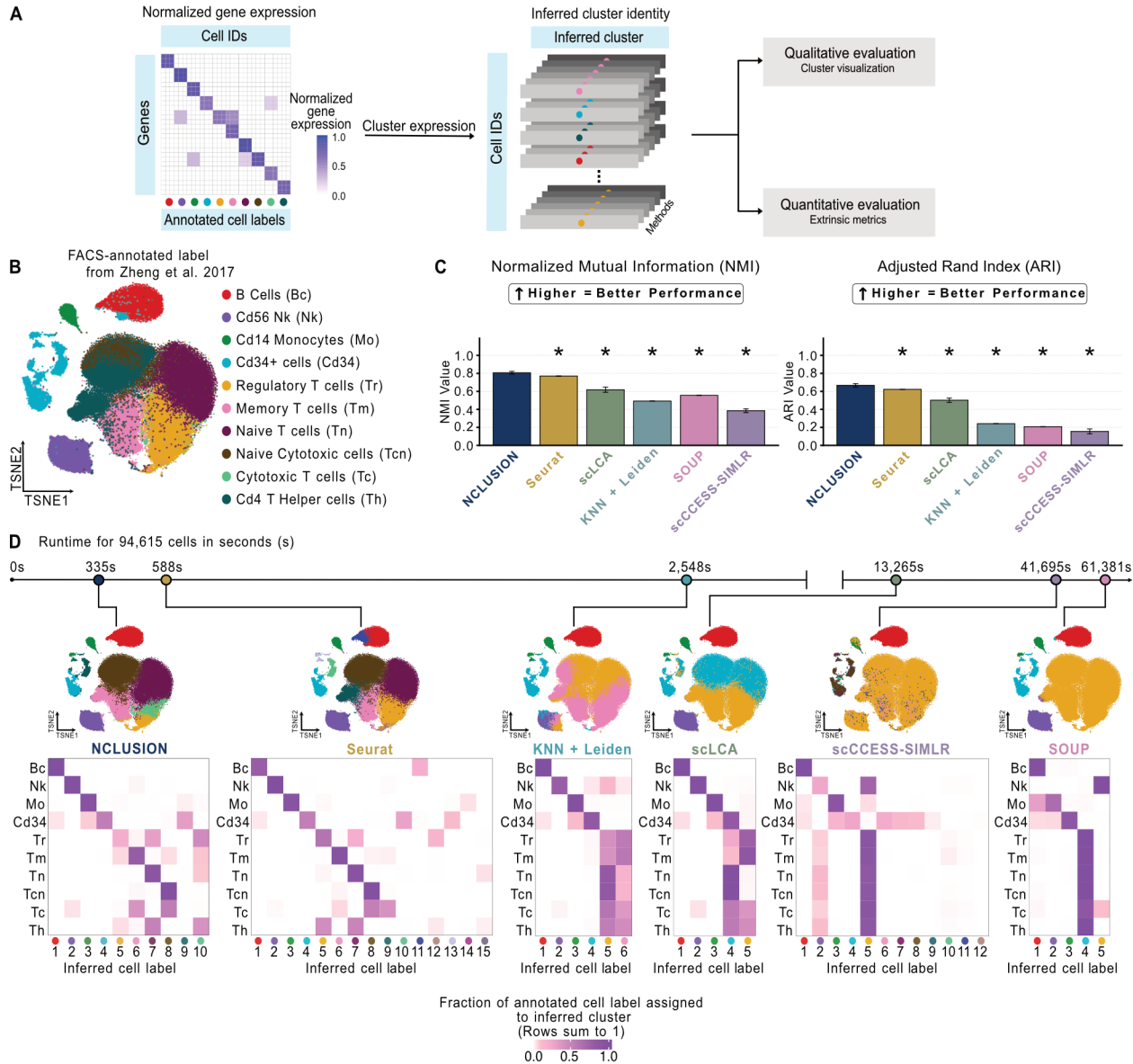


Fig 3. Clustering performance for NCLUSION and other baseline methods on the PBMC scRNA-seq dataset ($N = 94,615$ cells). (A) The framework used for evaluating the quality of clustering in each method. (B) Overview of FACS-based cell type annotations, visualized via t-distributed stochastic neighbor embedding (t-SNE), for the PBMC scRNA-seq dataset. These annotations serve as labels during the evaluation. (C) Assessment of the inferred cluster labels versus the experimental annotations, as quantified by two metrics: normalized mutual information (NMI) and adjusted Rand index (ARI) (for each method, we take five random 80% splits of the PBMC dataset; depicted in each bar plot is the mean \pm 95% confidence interval). Asterisks indicate that there is a statistically significant difference in performance between NCLUSION and a corresponding method (two-sided t-test $P < 0.05$). (D) Visualizing the structure of the inferred clusters across all baselines using t-SNEs and a contingency heat map showing the prevalence of each cell type within each cluster. Methods are ordered from fastest (left) to slowest (right) in terms of runtime. The same lower dimensional representation of the data is reused with relabeling of the plots according to the results from each clustering algorithm.

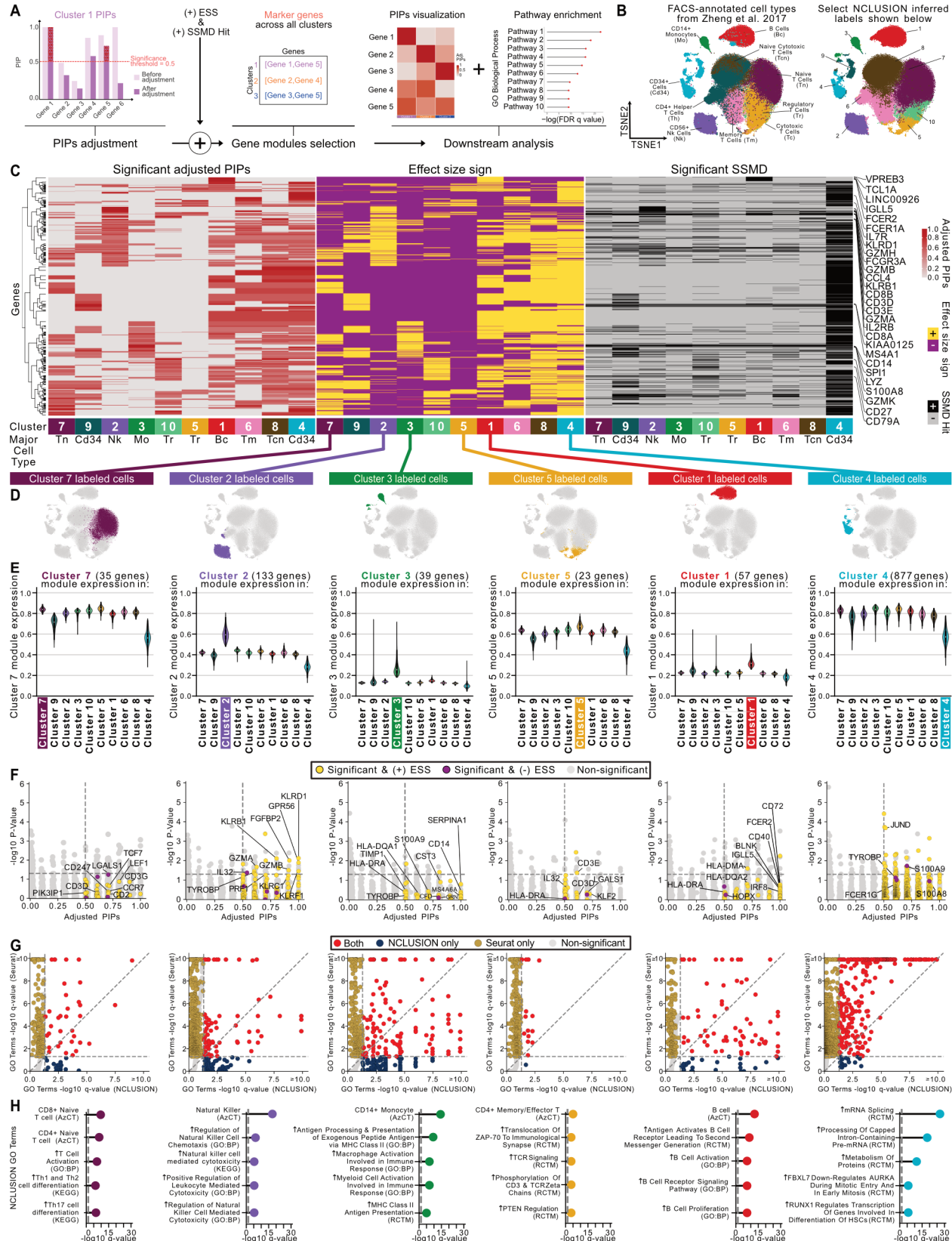


Fig 4. (Continued on the following page).

Fig 4. Evaluation of cluster-specific marker genes identified by NCLUSION on the PBMC dataset ($N = 94,615$ cells). (A) The framework used for assessing cluster-specific marker genes. (B) Embeddings of the experimental annotations for major cell types from the PBMC dataset compared to the clusters inferred by NCLUSION. (C) Heat maps of the adjusted posterior inclusion probabilities (PIPs) (left), effect size sign (ESS) (center), and strictly standardized mean difference (SSMD) (right) of significant genes in each cluster. Cluster-specific marker genes are selected as those that have a significant inclusion probability, are up-regulated in a given cluster, and have a large effect size magnitude such that $\text{PIP} \geq 0.5$, $\text{ESS} = +$, and $|\text{SSMD}(j; k)| \geq S^*(j; k)$, respectively. Here $S^*(j; k)$ is a threshold set to preserve a false positive rate of 0.05. (D) Highlighted location on t-SNEs of NCLUSION-inferred clusters that contain predominantly one cell type. (E) Violin plots comparing the normalized expression of cluster-specific marker genes in each of the inferred clusters. (F) Scatter plot comparing the marker genes identified using *post hoc* differential expression analysis with Seurat (yellow) versus the variable selection approach with NCLUSION (blue). Yellow points have $\text{PIP} \geq 0.5$ and $\text{ESS} = +$, while purple points have $\text{PIP} \geq 0.5$ and $\text{ESS} = -$, respectively. The vertical dashed line marks the median probability criterion³⁸, and the horizontal dashed line marks the Bonferroni-corrected threshold for significant q -values (i.e., an adjusted P). Genes in the top right quadrant are identified by both methods. (G) Scatter plot comparing gene ontology (GO) pathway enrichment analyses using cluster-specific marker genes from Seurat versus NCLUSION. The horizontal and vertical lines correspond to significant q -values being below 0.05. Pathways in the top right quadrant are selected by both approaches (red), while elements in the bottom right and top left quadrants are uniquely identified by NCLUSION (blue) and Seurat (orange), respectively. (H) Highlight of select top GO pathway enrichment analysis for the marker genes identified by NCLUSION. Plotted on the x-axis are the negative log-transformed q -values for each GO gene set. Gene sets with a q -value below 0.05 are deemed to be significant.



Fig 5. (Continued on the following page).

Fig 5. Scalability and generalizability of NCLUSION across diverse datasets. NCLUSION and baselines were applied to the following scRNA-seq datasets: PDAC ($N = 23,042$ cells)⁷², AML ($N = 43,690$ cells)⁷³, and IMMUNE ($N = 88,057$ cells)⁷⁴. **(A)** Runtimes for all methods when applied to each dataset. **(B)** Assessment of the inferred cluster labels from each method versus cell type annotations from the original studies. Evaluation is quantified by normalized mutual information (NMI) and adjusted Rand index (ARI). Asterisks indicate that there is a statistically significant difference in performance between NCLUSION and a corresponding method (two-sided t-test $P < 0.05$). Panels **(C)-(F)** depict results from running NCLUSION on the PDAC dataset. **(C)** Shown is a t-SNE visualization of the PDAC scRNA-seq dataset, annotated by the cell type labels from the PDAC study (top) compared to the clusters inferred by NCLUSION (bottom), where the “NM” labels indicate non-malignant cells and the “M” labels indicate malignant cells. **(D)** Heat maps of the adjusted posterior inclusion probabilities (PIPs) (left), effect size sign (ESS) (center), and strictly standardized mean difference (SSMD) (right) of the significant genes in each cluster. **(E)** Highlighted location on t-SNEs of NCLUSION-inferred clusters that contain predominantly one cell type. **(F)** Violin plots comparing the normalized expression of cluster-specific marker genes across clusters. **(G)** Gene ontology (GO) pathway enrichment analysis for the marker genes identified for each cluster. Gene sets with a q -value below 0.05 are deemed to be significant.

701 **References**

- 702 1. Zhen Miao, Benjamin D. Humphreys, Andrew P. McMahon, and Junhyong Kim. Multi-omics
703 integration in the age of million single-cell data. *Nature Reviews Nephrology*, 17(11):710–724,
704 November 2021. ISSN 1759-5061, 1759-507X. doi: 10.1038/s41581-021-00463-x.
- 705 2. F. Alexander Wolf, Philipp Angerer, and Fabian J. Theis. Scanpy: large-scale single-cell gene
706 expression data analysis. *Genome Biology*, 19(1):15, February 2018. ISSN 1474-760X. doi:
707 10.1186/s13059-017-1382-0.
- 708 3. Minzhe Guo, Hui Wang, S. Steven Potter, Jeffrey A. Whitsett, and Yan Xu. Sincera: A pipeline for
709 single-cell rna-seq profiling analysis. *PLOS Computational Biology*, 11(11):e1004575, November
710 2015. ISSN 1553-7358. doi: 10.1371/journal.pcbi.1004575.
- 711 4. Aaron T.L. Lun, Davis J. McCarthy, and John C. Marioni. A step-by-step workflow for low-level
712 analysis of single-cell rna-seq data with bioconductor. *F1000Research*, 5:2122, October 2016. ISSN
713 2046-1402. doi: 10.12688/f1000research.9501.2.
- 714 5. Ashraful Haque, Jessica Engel, Sarah A. Teichmann, and Tapio Lönberg. A practical guide to
715 single-cell rna-sequencing for biomedical research and clinical applications. *Genome Medicine*, 9
716 (1):75, August 2017. ISSN 1756-994X. doi: 10.1186/s13073-017-0467-4.
- 717 6. Oliver Stegle, Sarah A. Teichmann, and John C. Marioni. Computational and analytical challenges
718 in single-cell transcriptomics. *Nature Reviews Genetics*, 16(33):133–145, March 2015. ISSN 1471-
719 0064. doi: 10.1038/nrg3833.
- 720 7. Vladimir Yu Kiselev, Tallulah S. Andrews, and Martin Hemberg. Challenges in unsupervised
721 clustering of single-cell rna-seq data. *Nature Reviews Genetics*, 20(55):273–282, May 2019. ISSN
722 1471-0064. doi: 10.1038/s41576-018-0088-9.
- 723 8. Robert A. Amezquita, Aaron T. L. Lun, Etienne Becht, Vince J. Carey, Lindsay N. Carpp,
724 Ludwig Geistlinger, Federico Marini, Kevin Rue-Albrecht, Davide Risso, Charlotte Soneson, Levi
725 Waldron, Hervé Pagès, Mike L. Smith, Wolfgang Huber, Martin Morgan, Raphael Gottardo, and
726 Stephanie C. Hicks. Orchestrating single-cell analysis with bioconductor. *Nature Methods*, 17
727 (22):137–145, February 2020. ISSN 1548-7105. doi: 10.1038/s41592-019-0654-x.

728 9. Rahul Satija, Jeffrey A Farrell, David Gennert, Alexander F Schier, and Aviv Regev. Spatial
729 reconstruction of single-cell gene expression data. *Nature Biotechnology*, 33:495–502, 2015. doi:
730 10.1038/nbt.3192. URL <https://doi.org/10.1038/nbt.3192>.

731 10. Changde Cheng, John Easton, Celeste Rosencrance, Yan Li, Bensheng Ju, Justin Williams,
732 Heather L Mulder, Yakun Pang, Wenan Chen, and Xiang Chen. Latent cellular analysis ro-
733 bustly reveals subtle diversity in large-scale single-cell rna-seq data. *Nucleic Acids Research*, 47
734 (22):e143, Dec 2019. ISSN 0305-1048. doi: 10.1093/nar/gkz826.

735 11. Bo Wang, Junjie Zhu, Emma Pierson, Daniele Ramazzotti, and Serafim Batzoglou. Visualization
736 and analysis of single-cell rna-seq data by kernel-based similarity learning. *Nature Methods*, 14
737 (44):414–416, Apr 2017. ISSN 1548-7105. doi: 10.1038/nmeth.4207.

738 12. Laurens van der Maaten and Geoffrey Hinton. Visualizing data using t-sne. *Journal of Machine
739 Learning Research*, 9(86):2579–2605, 2008. ISSN 1533-7928.

740 13. Leland McInnes, John Healy, and James Melville. Umap: Uniform manifold approximation
741 and projection for dimension reduction, 2020. URL <http://arxiv.org/abs/1802.03426>.
742 arXiv:1802.03426 [cs, stat].

743 14. Romain Lopez, Jeffrey Regier, Michael B. Cole, Michael I. Jordan, and Nir Yosef. Deep generative
744 modeling for single-cell transcriptomics. *Nature Methods*, 15(12):1053–1058, Dec 2018. ISSN
745 1548-7091, 1548-7105. doi: 10.1038/s41592-018-0229-2.

746 15. Vladimir Yu Kiselev, Kristina Kirschner, Michael T. Schaub, Tallulah Andrews, Andrew Yiu,
747 Tamir Chandra, Kedar N. Natarajan, Wolf Reik, Mauricio Barahona, Anthony R. Green, and
748 Martin Hemberg. Sc3: consensus clustering of single-cell rna-seq data. *Nature Methods*, 14(55):
749 483–486, May 2017. ISSN 1548-7105. doi: 10.1038/nmeth.4236.

750 16. Dominic Grün, Anna Lyubimova, Lennart Kester, Kay Wiebrands, Onur Basak, Nobuo Sasaki,
751 Hans Clevers, and Alexander van Oudenaarden. Single-cell messenger rna sequencing reveals rare
752 intestinal cell types. *Nature*, 525(75687568):251–255, September 2015. ISSN 1476-4687. doi:
753 10.1038/nature14966.

754 17. Bosiljka Tasic, Vilas Menon, Thuc Nghi Nguyen, Tae Kyung Kim, Tim Jarsky, Zizhen Yao, Boaz
755 Levi, Lucas T. Gray, Staci A. Sorensen, Tim Dolbeare, Darren Bertagnolli, Jeff Goldy, Nadiya
756 Shapovalova, Sheana Parry, Changkyu Lee, Kimberly Smith, Amy Bernard, Linda Madisen, Su-
757 san M. Sunkin, Michael Hawrylycz, Christof Koch, and Hongkui Zeng. Adult mouse cortical cell
758 taxonomy revealed by single cell transcriptomics. *Nature Neuroscience*, 19(22):335–346, February
759 2016. ISSN 1546-1726. doi: 10.1038/nn.4216.

760 18. Justina žurauskienė and Christopher Yau. pcareduce: hierarchical clustering of single cell
761 transcriptional profiles. *BMC Bioinformatics*, 17(1):140, March 2016. ISSN 1471-2105. doi:
762 10.1186/s12859-016-0984-y.

763 19. Amit Zeisel, Ana B. Muñoz-Manchado, Simone Codeluppi, Peter Lönnerberg, Gioele La Manno,
764 Anna Juréus, Sueli Marques, Hermany Munguba, Liqun He, Christer Betsholtz, Charlotte Rolny,
765 Gonçalo Castelo-Branco, Jens Hjerling-Leffler, and Sten Linnarsson. Cell types in the mouse
766 cortex and hippocampus revealed by single-cell rna-seq. *Science*, 347(6226):1138–1142, March
767 2015. doi: 10.1126/science.aaa1934.

768 20. Malte D Luecken and Fabian J Theis. Current best practices in single-cell rna-seq analysis: a
769 tutorial. *Molecular Systems Biology*, 15(6):e8746, Jun 2019. ISSN 1744-4292. doi: 10.15252/msb
770 .20188746.

771 21. David Lähnemann, Johannes Köster, Ewa Szczurek, Davis J. McCarthy, Stephanie C. Hicks,
772 Mark D. Robinson, Catalina A. Vallejos, Kieran R. Campbell, Niko Beerenwinkel, Ahmed Mah-
773 foulz, Luca Pinello, Pavel Skums, Alexandros Stamatakis, Camille Stephan-Otto Attolini, Samuel
774 Aparicio, Jasmijn Baaijens, Marleen Balvert, Buys de Barbanson, Antonio Cappuccio, Gia-
775 como Corleone, Bas E. Dutilh, Maria Florescu, Victor Guryev, Rens Holmer, Katharina Jahn,
776 Thamar Jessurun Lobo, Emma M. Keizer, Indu Khatri, Szymon M. Kielbasa, Jan O. Korbel,
777 Alexey M. Kozlov, Tzu-Hao Kuo, Boudewijn P.F. Lelieveldt, Ion I. Mandoiu, John C. Marioni,
778 Tobias Marschall, Felix Mölder, Amir Niknejad, Lukasz Raczkowski, Marcel Reinders, Jeroen de
779 Ridder, Antoine-Emmanuel Saliba, Antonios Somarakis, Oliver Stegle, Fabian J. Theis, Huan
780 Yang, Alex Zelikovsky, Alice C. McHardy, Benjamin J. Raphael, Sohrab P. Shah, and Alexander
781 Schönhuth. Eleven grand challenges in single-cell data science. *Genome Biology*, 21(1):31, Feb
782 2020. ISSN 1474-760X. doi: 10.1186/s13059-020-1926-6.

783 22. Lucy L. Gao, Jacob Bien, and Daniela Witten. Selective inference for hierarchical clustering.
784 Journal of the American Statistical Association, page 2116331, October 2022. ISSN 0162-1459,
785 1537-274X. doi: 10.1080/01621459.2022.2116331. Web of Science ID: WOS:000866074100001.

786 23. Anna Neufeld, Lucy L. Gao, Joshua Popp, Alexis Battle, and Daniela Witten. Inference af-
787 ter latent variable estimation for single-cell rna sequencing data. Biostatistics, December 2022.
788 ISSN 1465-4644, 1468-4357. doi: 10.1093/biostatistics/kxac047. Web of Science ID:
789 WOS:000896827000001.

790 24. Isabella N. Grabski, Kelly Street, and Rafael A. Irizarry. Significance analysis for clustering with
791 single-cell rna-sequencing data. Nature Methods, 20(88):1196–1202, Aug 2023. ISSN 1548-7105.
792 doi: 10.1038/s41592-023-01933-9.

793 25. Alexis Vandenbon and Diego Diez. A clustering-independent method for finding differentially
794 expressed genes in single-cell transcriptome data. Nature Communications, 11(11):4318, August
795 2020. ISSN 2041-1723. doi: 10.1038/s41467-020-17900-3.

796 26. Jesse M Zhang, Govinda M Kamath, and N Tse David. Valid post-clustering differential analysis
797 for single-cell rna-seq. Cell Systems, 9(4):383–392, 2019.

798 27. Alan DenAdel, Michelle L. Ramseier, Andrew W. Navia, Alex K. Shalek, Srivatsan Raghavan,
799 Peter S. Winter, Ava P. Amini, and Lorin Crawford. Artificial variables help to avoid over-
800 clustering in single-cell rna sequencing. The American Journal of Human Genetics, 0(0), March
801 2025. ISSN 0002-9297, 1537-6605. doi: 10.1016/j.ajhg.2025.02.014. URL [https://www.cell.com/ajhg/abstract/S0002-9297\(25\)00061-8](https://www.cell.com/ajhg/abstract/S0002-9297(25)00061-8).

803 28. Jesse M Zhang, Jue Fan, H Christina Fan, David Rosenfeld, and David N Tse. An interpretable
804 framework for clustering single-cell rna-seq datasets. BMC bioinformatics, 19(1):1–12, 2018.

805 29. Snehalika Lall, Sumanta Ray, and Sanghamitra Bandyopadhyay. Rgcop-a regularized copula
806 based method for gene selection in single-cell rna-seq data. PLOS Computational Biology, 17
807 (10):e1009464, 2021.

808 30. F William Townes, Stephanie C Hicks, Martin J Aryee, and Rafael A Irizarry. Feature selection

809 and dimension reduction for single-cell rna-seq based on a multinomial model. *Genome Biology*,
810 20:1–16, 2019.

811 31. David M. Blei and Michael I. Jordan. Variational inference for dirichlet process mixtures. *Bayesian*
812 *Analysis*, 1(1):121–143, Mar 2006. ISSN 1936-0975, 1931-6690. doi: 10.1214/06-BA104.

813 32. Andrew Gelman, John B Carlin, Hal S Stern, David B Dunson, Aki Vehtari, and Donald B Rubin.
814 *Bayesian Data Analysis, Third Edition*. CRC Press, Hoboken, 2013. ISBN 978-1-4398-9820-8.

815 33. Sandhya Prabhakaran, Elham Azizi, Ambrose Carr, and Dana Pe'er. Dirichlet process mixture
816 model for correcting technical variation in single-cell gene expression data. *JMLR Workshop and*
817 *Conference Proceedings*, 48:1070–1079, 2016. ISSN 1938-7288.

818 34. Zhe Sun, Li Chen, Hongyi Xin, Yale Jiang, Qianhui Huang, Anthony R Cillo, Tracy Tabib, Jay K
819 Kolls, Tullia C Bruno, Robert Lafyatis, et al. A bayesian mixture model for clustering droplet-
820 based single-cell transcriptomic data from population studies. *Nature communications*, 10(1):
821 1649, 2019.

822 35. Tiehang Duan, José P Pinto, and Xiaohui Xie. Parallel clustering of single cell transcriptomic data
823 with split-merge sampling on dirichlet process mixtures. *Bioinformatics*, 35(6):953–961, 2019.

824 36. Zhe Sun, Ting Wang, Ke Deng, Xiao-Feng Wang, Robert Lafyatis, Ying Ding, Ming Hu, and Wei
825 Chen. Dimm-sc: a dirichlet mixture model for clustering droplet-based single cell transcriptomic
826 data. *Bioinformatics*, 34(1):139–146, 2018.

827 37. Nigatu A. Adossa, Kalle T. Rytkönen, and Laura L. Elo. Dirichlet process mixture models for
828 single-cell rna-seq clustering. *Biology Open*, 11(4):bio059001, April 2022. ISSN 2046-6390. doi:
829 10.1242/bio.059001. Citation Key: adossaDirichletProcessMixture2022.

830 38. Maria Maddalena Barbieri and James O. Berger. Optimal predictive model selection. *The Annals*
831 *of Statistics*, 32(3):870–897, Jun 2004. ISSN 0090-5364, 2168-8966. doi: 10.1214/00905360400000
832 0238.

833 39. Ping Zeng and Xiang Zhou. Non-parametric genetic prediction of complex traits with latent
834 dirichlet process regression models. *Nature Communications*, 8(1):456, Dec 2017. ISSN 2041-
835 1723. doi: 10.1038/s41467-017-00470-2.

836 40. Peter Carbonetto and Matthew Stephens. Scalable variational inference for bayesian variable
837 selection in regression, and its accuracy in genetic association studies. *Bayesian Analysis*, 7:
838 73–108, Mar 2012. ISSN 1936-0975, 1931-6690. doi: 10.1214/12-BA703.

839 41. Pinar Demetci, Wei Cheng, Gregory Darnell, Xiang Zhou, Sohini Ramachandran, and Lorin
840 Crawford. Multi-scale inference of genetic trait architecture using biologically annotated neural
841 networks. *PLOS Genetics*, 17(8):e1009754, 2021. ISSN 1553-7404. doi: 10.1371/journal.pgen.100
842 9754.

843 42. David M. Blei, Alp Kucukelbir, and Jon D. McAuliffe. Variational inference: A review for statis-
844 ticians. *Journal of the American Statistical Association*, 112(518):859–877, April 2017. ISSN
845 0162-1459, 1537-274X. doi: 10.1080/01621459.2017.1285773. tex.ids: bleiVariationalInferenceRe-
846 view2017a arXiv: 1601.00670.

847 43. F. Pedregosa, G. Varoquaux, A. Gramfort, V. Michel, B. Thirion, O. Grisel, M. Blondel, P. Pret-
848 tenhofer, R. Weiss, V. Dubourg, J. Vanderplas, A. Passos, D. Cournapeau, M. Brucher, M. Per-
849 rot, and E. Duchesnay. Scikit-learn: Machine learning in Python. *Journal of Machine Learning
850 Research*, 12:2825–2830, 2011.

851 44. Lingxue Zhu, Jing Lei, Lambertus Klei, Bernie Devlin, and Kathryn Roeder. Semisoft clustering
852 of single-cell data. *Proceedings of the National Academy of Sciences*, 116(2):466–471, Jan 2019.
853 doi: 10.1073/pnas.1817715116.

854 45. 10x Genomics. Support: single cell gene expression datasets, 2023. URL <https://www.10xgenomics.com/resources/datasets>.

855 46. Valentine Svensson, Eduardo da Veiga Beltrame, and Lior Pachter. A curated database reveals
856 trends in single-cell transcriptomics. *Database: The Journal of Biological Databases and Curation*,
857 2020:baaa073, Nov 2020. ISSN 1758-0463. doi: 10.1093/database/baaa073.

858 47. Dongyuan Song, Qingyang Wang, Guanao Yan, Tianyang Liu, Tianyi Sun, and Jingyi Jessica Li.
859 scdesign3 generates realistic in silico data for multimodal single-cell and spatial omics. *Nature
860 Biotechnology*, page 1–6, May 2023. ISSN 1546-1696. doi: 10.1038/s41587-023-01772-1.

862 48. Peijie Lin, Michael Troup, and Joshua W. K. Ho. Cidr: Ultrafast and accurate clustering through
863 imputation for single-cell rna-seq data. *Genome Biology*, 18(1):59, March 2017. ISSN 1474-760X.
864 doi: 10.1186/s13059-017-1188-0.

865 49. Vladimir Yu Kiselev, Kristina Kirschner, Michael T. Schaub, Tallulah Andrews, Andrew Yiu,
866 Tamir Chandra, Kedar N. Natarajan, Wolf Reik, Mauricio Barahona, Anthony R. Green, and
867 Martin Hemberg. Sc3: consensus clustering of single-cell rna-seq data. *Nature Methods*, 14(55):
868 483–486, May 2017. ISSN 1548-7105. doi: 10.1038/nmeth.4236.

869 50. Tian Tian, Ji Wan, Qi Song, and Zhi Wei. Clustering single-cell rna-seq data with a model-based
870 deep learning approach. *Nature Machine Intelligence*, 1(44):191–198, April 2019. ISSN 2522-5839.
871 doi: 10.1038/s42256-019-0037-0.

872 51. Bobby Ranjan, Wenjie Sun, Jinyu Park, Kunal Mishra, Florian Schmidt, Ronald Xie, Fatemeh
873 Alipour, Vipul Singhal, Ignasius Joanito, Mohammad Amin Honardoost, Jacy Mei Yun Yong,
874 Ee Tzun Koh, Khai Pang Leong, Nirmala Arul Rayan, Michelle Gek Liang Lim, and Shyam
875 Prabhakar. DubstepR is a scalable correlation-based feature selection method for accurately clus-
876 tering single-cell data. *Nature Communications*, 12(1):5849, October 2021. ISSN 2041-1723. doi:
877 10.1038/s41467-021-26085-2. Citation Key: ranjanDUBStepRScalableCorrelationbased2021.

878 52. Zihao Chen, Changhu Wang, Siyuan Huang, Yang Shi, and Ruibin Xi. Directly selecting cell-type
879 marker genes for single-cell clustering analyses. *Cell Reports Methods*, 4(7):100810, July 2024.
880 ISSN 26672375. doi: 10.1016/j.crmeth.2024.100810. Citation Key: chenDirectlySelectingCell-
881 type2024.

882 53. Grace X. Y. Zheng, Jessica M. Terry, Phillip Belgrader, Paul Ryvkin, Zachary W. Bent, Ryan
883 Wilson, Solongo B. Ziraldo, Tobias D. Wheeler, Geoff P. McDermott, Junjie Zhu, Mark T. Gre-
884 gory, Joe Shuga, Luz Montesclaros, Jason G. Underwood, Donald A. Masquelier, Stefanie Y.
885 Nishimura, Michael Schnall-Levin, Paul W. Wyatt, Christopher M. Hindson, Rajiv Bharadwaj,
886 Alexander Wong, Kevin D. Ness, Lan W. Beppu, H. Joachim Deeg, Christopher McFarland,
887 Keith R. Loeb, William J. Valente, Nolan G. Ericson, Emily A. Stevens, Jerald P. Radich, Tarjei S.
888 Mikkelsen, Benjamin J. Hindson, and Jason H. Bielas. Massively parallel digital transcriptional

889 profiling of single cells. *Nature Communications*, 8(11):14049, Jan 2017. ISSN 2041-1723. doi:
890 10.1038/ncomms14049.

891 54. Alexander HS Vargo and Anna C Gilbert. A rank-based marker selection method for high through-
892 put scRNA-seq data. *BMC bioinformatics*, 21(1):1–51, 2020.

893 55. Lieke Michielsen, Marcel J. T. Reinders, and Ahmed Mahfouz. Hierarchical progressive learning
894 of cell identities in single-cell data. *Nature Communications*, 12(11):2799, May 2021. ISSN 2041-
895 1723. doi: 10.1038/s41467-021-23196-8.

896 56. Daniel M. Baume, Michael A. Caligiuri, Thomas J. Manley, John F. Daley, and Jerome Ritz.
897 Differential expression of CD8 α and CD8 β associated with MHC-restricted and non-MHC-restricted
898 cytolytic effector cells. *Cellular Immunology*, 131(2):352–365, December 1990. ISSN 0008-8749.
899 doi: 10.1016/0008-8749(90)90260-X.

900 57. Jenny Hendriks, Loes A. Gravestein, Kiki Tesselaar, René A. W. van Lier, Ton N. M. Schumacher,
901 and Jannie Borst. CD27 is required for generation and long-term maintenance of T cell immunity.
902 *Nature Immunology*, 1(5):433–440, November 2000. ISSN 1529-2916. doi: 10.1038/80877.

903 58. Suzanne Norris, Derek G. Doherty, Clive Collins, Gerry McEntee, Oscar Traynor, John E. Hegarty,
904 and Cliona O’Farrelly. Natural T cells in the human liver: cytotoxic lymphocytes with dual T cell
905 and natural killer cell phenotype and function are phenotypically heterogeneous and include V α 24-
906 j α q and γ δ T cell receptor bearing cells. *Human Immunology*, 60(1):20–31, Jan 1999. ISSN
907 0198-8859. doi: 10.1016/S0198-8859(98)00098-6.

908 59. Simon N. Willis, Julie Tellier, Yang Liao, Stephanie Trezise, Amanda Light, Kristy O’Donnell,
909 Lee Ann Garrett-Sinha, Wei Shi, David M. Tarlinton, and Stephen L. Nutt. Environmental sensing
910 by mature B cells is controlled by the transcription factors pu.1 and spib. *Nature Communications*,
911 8(11):1426, November 2017. ISSN 2041-1723. doi: 10.1038/s41467-017-01605-1.

912 60. Jonathan Zuccolo, Lili Deng, Tammy Unruh, Ratna Sanyal, Jeremy Bau, Jan Storek, Douglas
913 Demetrick, Joanne Luider, Iwona Auer-Grzesiak, Adnan Mansoor, and Julie Deans. Expression
914 of MS4A and TMEM176 genes in human B lymphocytes. *Frontiers in Immunology*, 4, 2013. ISSN
915 1664-3224. URL <https://www.frontiersin.org/articles/10.3389/fimmu.2013.00195>.

916 61. Zheng Chen, Mincheng Yu, Jiuliang Yan, Lei Guo, Bo Zhang, Shuang Liu, Jin Lei, Wen-
917 tao Zhang, Binghai Zhou, Jie Gao, Zhangfu Yang, Xiaoqiang Li, Jian Zhou, Jia Fan, Qing-
918 hai Ye, Hui Li, Yongfeng Xu, and Yongsheng Xiao. Pnoc expressed by b cells in cholan-
919 giocarcinoma was survival related and lair2 could be a t cell exhaustion biomarker in tu-
920 mor microenvironment: Characterization of immune microenvironment combining single-cell
921 and bulk sequencing technology. *Frontiers in Immunology*, 12, 2021. ISSN 1664-3224. URL
922 <https://www.frontiersin.org/articles/10.3389/fimmu.2021.647209>.

923 62. Elza Evren, Emma Ringqvist, Kumar Parijat Tripathi, Natalie Sleiers, Inés Có Rives, Arlisa Al-
924 isjahbana, Yu Gao, Dhifaf Sarhan, Tor Halle, Chiara Sorini, Rico Lepzien, Nicole Marquardt,
925 Jakob Michaëlsson, Anna Smed-Sörensen, Johan Botling, Mikael C.I. Karlsson, Eduardo J. Vil-
926 lablanca, and Tim Willinger. Distinct developmental pathways from blood monocytes generate
927 human lung macrophage diversity. *Immunity*, 54(2):259–275.e7, February 2021. ISSN 10747613.
928 doi: 10.1016/j.jimmuni.2020.12.003.

929 63. Zhuoqing Fang, Xinyuan Liu, and Gary Peltz. Gseapy: a comprehensive package for performing
930 gene set enrichment analysis in python. *Bioinformatics*, 39(1):btac757, January 2023. ISSN 1367-
931 4811. doi: 10.1093/bioinformatics/btac757.

932 64. Steffen Durinck, Yves Moreau, Arek Kasprzyk, Sean Davis, Bart De Moor, Alvis Brazma, and
933 Wolfgang Huber. Biomart and bioconductor: a powerful link between biological databases and
934 microarray data analysis. *Bioinformatics*, 21(16):3439–3440, August 2005. ISSN 1367-4803. doi:
935 10.1093/bioinformatics/bti525.

936 65. Edward Y. Chen, Christopher M. Tan, Yan Kou, Qiaonan Duan, Zichen Wang, Gabriela Vaz
937 Meirelles, Neil R. Clark, and Avi Ma'ayan. Enrichr: interactive and collaborative html5 gene
938 list enrichment analysis tool. *BMC Bioinformatics*, 14:128, April 2013. ISSN 1471-2105. doi:
939 10.1186/1471-2105-14-128.

940 66. Michael Ashburner, Catherine A. Ball, Judith A. Blake, David Botstein, Heather Butler,
941 J. Michael Cherry, Allan P. Davis, Kara Dolinski, Selina S. Dwight, Janan T. Eppig, Midori A.
942 Harris, David P. Hill, Laurie Issel-Tarver, Andrew Kasarskis, Suzanna Lewis, John C. Matese,
943 Joel E. Richardson, Martin Ringwald, Gerald M. Rubin, and Gavin Sherlock. Gene ontology:

944 tool for the unification of biology. *Nature Genetics*, 25(11):25–29, May 2000. ISSN 1546-1718.
945 doi: 10.1038/75556.

946 67. Seth Carbon and Chris Mungall. Gene ontology data archive, Jul 2023. URL <https://zenodo.org/record/8200914>.

948 68. Eric Vivier, Elena Tomasello, Myriam Baratin, Thierry Walzer, and Sophie Ugolini. Functions
949 of natural killer cells. *Nature Immunology*, 9(55):503–510, May 2008. ISSN 1529-2916. doi:
950 10.1038/ni1582.

951 69. Sourav Paul and Girdhari Lal. The molecular mechanism of natural killer cells function and its
952 importance in cancer immunotherapy. *Frontiers in Immunology*, 8, 2017. ISSN 1664-3224. URL
953 <https://www.frontiersin.org/articles/10.3389/fimmu.2017.01124>.

954 70. Baptiste N. Jaeger, Jean Donadieu, Céline Cognet, Claire Bernat, Diana Ordoñez-Rueda, Vincent
955 Barlogis, Nizar Mahlaoui, Aurore Fenis, Emilie Narni-Mancinelli, Blandine Beaupain, Christine
956 Bellanné-Chantelot, Marc Bajéhoff, Bernard Malissen, Marie Malissen, Eric Vivier, and Sophie
957 Ugolini. Neutrophil depletion impairs natural killer cell maturation, function, and homeostasis.
958 *The Journal of Experimental Medicine*, 209(3):565–580, March 2012. ISSN 0022-1007. doi: 10.1
959 084/jem.20111908.

960 71. Kun Jiang, Bin Zhong, Danielle L. Gilvary, Brian C. Corliss, Elizabeth Hong-Geller, Sheng Wei,
961 and Julie Y. Djeu. Pivotal role of phosphoinositide-3 kinase in regulation of cytotoxicity in
962 natural killer cells. *Nature Immunology*, 1(55):419–425, November 2000. ISSN 1529-2916. doi:
963 10.1038/80859.

964 72. Srivatsan Raghavan, Peter S. Winter, Andrew W. Navia, Hannah L. Williams, Alan DenAdel,
965 Kristen E. Lowder, Jennyfer Galvez-Reyes, Radha L. Kalekar, Nolawit Mulugeta, Kevin S. Kap-
966 ner, Manisha S. Raghavan, Ashir A. Borah, Nuo Liu, Sara A. Väyrynen, Andressa Dias Costa,
967 Raymond W. S. Ng, Junning Wang, Emma K. Hill, Dorisanne Y. Ragon, Lauren K. Brais, Alex M.
968 Jaeger, Liam F. Spurr, Yvonne Y. Li, Andrew D. Cherniack, Matthew A. Booker, Elizabeth F.
969 Cohen, Michael Y. Tolstorukov, Isaac Wakiro, Asaf Rotem, Bruce E. Johnson, James M. McFar-
970 land, Ewa T. Sicinska, Tyler E. Jacks, Ryan J. Sullivan, Geoffrey I. Shapiro, Thomas E. Clancy,
971 Kimberly Perez, Douglas A. Rubinson, Kimmie Ng, James M. Cleary, Lorin Crawford, Scott R.

972 Manalis, Jonathan A. Nowak, Brian M. Wolpin, William C. Hahn, Andrew J. Aguirre, and Alex K.
973 Shalek. Microenvironment drives cell state, plasticity, and drug response in pancreatic cancer.
974 Cell, 184(25):6119–6137.e26, Dec 2021. ISSN 0092-8674. doi: 10.1016/j.cell.2021.11.017.

975 73. Peter van Galen, Volker Hovestadt, Marc H. Wadsworth II, Travis K. Hughes, Gabriel K. Griffin,
976 Sofia Battaglia, Julia A. Verga, Jason Stephansky, Timothy J. Pastika, Jennifer Lombardi Story,
977 Geraldine S. Pinkus, Olga Pozdnyakova, Ilene Galinsky, Richard M. Stone, Timothy A. Graubert,
978 Alex K. Shalek, Jon C. Aster, Andrew A. Lane, and Bradley E. Bernstein. Single-cell rna-seq
979 reveals aml hierarchies relevant to disease progression and immunity. Cell, 176(6):1265–1281.e24,
980 Mar 2019. ISSN 00928674. doi: 10.1016/j.cell.2019.01.031. tex.ids: vangalenSingleCellRNASE-
981 qReveals2019a.

982 74. C. Domínguez Conde, C. Xu, L. B. Jarvis, D. B. Rainbow, S. B. Wells, T. Gomes, S. K. Howlett,
983 O. Suchanek, K. Polanski, H. W. King, L. Mamanova, N. Huang, P. A. Szabo, L. Richardson,
984 L. Bolt, E. S. Fasouli, K. T. Mahbubani, M. Prete, L. Tuck, N. Richoz, Z. K. Tuong, L. Campos,
985 H. S. Mousa, E. J. Needham, S. Pritchard, T. Li, R. Elmentait, J. Park, E. Rahmani, D. Chen,
986 D. K. Menon, O. A. Bayraktar, L. K. James, K. B. Meyer, N. Yosef, M. R. Clatworthy, P. A.
987 Sims, D. L. Farber, K. Saeb-Parsy, J. L. Jones, and S. A. Teichmann. Cross-tissue immune cell
988 analysis reveals tissue-specific features in humans. Science, 376(6594):eabl5197, May 2022. doi:
989 10.1126/science.abl5197.

990 75. Mazen Almehmadi, Brian F. Flanagan, Naeem Khan, Suliman Alomar, and Stephen E. Christmas.
991 Increased numbers and functional activity of cd56+ t cells in healthy cytomegalovirus positive
992 subjects. Immunology, 142(2):258, April 2014. doi: 10.1111/imm.12250.

993 76. Emily R. Kansler and Ming O. Li. Innate lymphocytes—lineage, localization and timing of
994 differentiation. Cellular and Molecular Immunology, 16(7):627–633, July 2019. ISSN 1672-7681.
995 doi: 10.1038/s41423-019-0211-7.

996 77. L. Beviglia and R. H. Kramer. Hgf induces fak activation and integrin-mediated adhesion in mtln3
997 breast carcinoma cells. International Journal of Cancer, 83(5):640–649, November 1999. ISSN
998 0020-7136. doi: 10.1002/(sici)1097-0215(19991126)83:5<640::aid-ijc13>3.0.co;2-d.

999 78. Tobias Silzle, Gwendalyn J. Randolph, Marina Kreutz, and Leoni A. Kunz-Schughart. The fi-
1000 broblast: Sentinel cell and local immune modulator in tumor tissue. International Journal of
1001 Cancer, 108(2):173–180, 2004. ISSN 1097-0215. doi: 10.1002/ijc.11542.

1002 79. Serena Meraviglia, Paola Di Carlo, Diego Pampinella, Giuliana Guadagnino, Elena Lo Presti,
1003 Valentina Orlando, Giulia Marchetti, Francesco Dieli, and Consolato Sergi. T-cell subsets (tcm,
1004 tem, temra) and poly-functional immune response in patients with human immunodeficiency virus
1005 (hiv) infection and different t-cd4 cell response. Annals of Clinical & Laboratory Science, 49(4):
1006 519–528, 2019. ISSN 0091-7370, 1550-8080.

1007 80. Jason M. Schenkel and David Masopust. Tissue-resident memory t cells. Immunity, 41(6):886–897,
1008 December 2014. ISSN 1074-7613. doi: 10.1016/j.immuni.2014.12.007.

1009 81. Michael M. Opata, Samad A. Ibitokou, Victor H. Carpio, Karis M. Marshall, Brian E. Dillon,
1010 Jordan C. Carl, Kyle D. Wilson, Christine M. Arcari, and Robin Stephens. Protection by and
1011 maintenance of cd4 effector memory and effector t cell subsets in persistent malaria infection.
1012 PLOS Pathogens, 14(4):e1006960, 2018. ISSN 1553-7374. doi: 10.1371/journal.ppat.1006960.

1013 82. Shane Crotty. T follicular helper cell differentiation, function, and roles in disease. Immunity, 41
1014 (4):529–542, October 2014. ISSN 1074-7613. doi: 10.1016/j.immuni.2014.10.004.

1015 83. Dimitrios V. Vavoulis, Margherita Francescatto, Peter Heutink, and Julian Gough. Dgeclust:
1016 differential expression analysis of clustered count data. Genome Biology, 16(1):39, February
1017 2015. ISSN 1465-6906. doi: 10.1186/s13059-015-0604-6.

1018 84. Charlotte Soneson and Mark D. Robinson. Bias, robustness and scalability in single-cell differential
1019 expression analysis. Nature Methods, 15(44):255–261, April 2018. ISSN 1548-7105. doi: 10.103
1020 8/nmeth.4612.

1021 85. Constantin Ahlmann-Eltze and Wolfgang Huber. Comparison of transformations for single-cell
1022 rna-seq data. Nature Methods, Apr 2023. ISSN 1548-7091, 1548-7105. doi: 10.1038/s41592-023
1023 -01814-1. URL <https://www.nature.com/articles/s41592-023-01814-1>.

1024 86. Xiang Zhu and Matthew Stephens. Large-scale genome-wide enrichment analyses identify new

1025 trait-associated genes and pathways across 31 human phenotypes. *Nature Communications*, 9(1):
1026 4361, 2018.

1027 87. Ying Ma, Shiquan Sun, Xuequn Shang, Evan T Keller, Mengjie Chen, and Xiang Zhou. Integrative
1028 differential expression and gene set enrichment analysis using summary statistics for scRNA-seq
1029 studies. *Nature Communications*, 11(1):1585, 2020.

1030 88. Jacob Bien and Robert J. Tibshirani. Sparse estimation of a covariance matrix. *Biometrika*, 98
1031 (4):807–820, December 2011. ISSN 0006-3444. doi: 10.1093/biomet/asr054.

1032 89. Youssef M Aboutaleb, Mazen Danaf, Yifei Xie, and Moshe E Ben-Akiva. Sparse covariance
1033 estimation in logit mixture models. *The Econometrics Journal*, 24(3):377–398, September 2021.
1034 ISSN 1368-4221. doi: 10.1093/ectj/utab008.

1035 90. David M Blei, Alp Kucukelbir, and Jon D McAuliffe. Variational inference: A review for statis-
1036 ticians. *Journal of the American Statistical Association*, 112(518):859–877, 2017.

1037 91. Ryan Giordano, Tamara Broderick, and Michael I Jordan. Covariances, robustness and variational
1038 bayes. *Journal of Machine Learning Research*, 19(51), 2018.

1039 92. Cheng Zhang, Babak Shahbaba, and Hongkai Zhao. Variational hamiltonian monte carlo via score
1040 matching. *Bayesian Analysis*, 13(2):485, 2018.

1041 93. Lukas M Weber, Arkajyoti Saha, Abhirup Datta, Kasper D Hansen, and Stephanie C Hicks.
1042 nmsvg for the scalable identification of spatially variable genes using nearest-neighbor gaussian
1043 processes. *Nature Communications*, 14(1):4059, 2023.

1044 94. Brian J Reich and Howard D Bondell. A spatial dirichlet process mixture model for clustering
1045 population genetics data. *Biometrics*, 67(2):381–390, 2011.

1046 95. Yongtao Guan and Matthew Stephens. Bayesian variable selection regression for genome-wide
1047 association studies and other large-scale problems. *The Annals of Applied Statistics*, 5(3):1780–1815,
1048 2011. doi: 10.1214/11-AOAS455. URL <https://projecteuclid.org:443/euclid.aoas/1318514285>.

1049 96. Xiang Zhou, Peter Carbonetto, and Matthew Stephens. Polygenic modeling with Bayesian sparse
1050 linear mixed models. *PLOS Genetics*, 9(2):e1003264, 2013.

1051

1052 97. Xiang Zhu and Matthew Stephens. Bayesian large-scale multiple regression with summary statistics from genome-wide association studies. *The Annals Applied Statistics*, 11(3):1561–1592, 2017.
1053 doi: 10.1214/17-AOAS1046. URL <https://projecteuclid.org:443/euclid.aoas/1507168840>.

1054 98. Michael C Hughes, Dae Il Kim, and Erik B Sudderth. Reliable and scalable variational inference
1055 for the hierarchical dirichlet process. *Artificial Intelligence and Statistics*, page 9, 2015.

1056 99. Jacob Cohen. *Statistical Power Analysis for the Behavioral Sciences*. Academic press, 2013.

1059 100. Xiaohua Douglas Zhang. A pair of new statistical parameters for quality control in rna interference
1060 high-throughput screening assays. *Genomics*, 89(4):552–561, April 2007. ISSN 0888-7543. doi:
1061 10.1016/j.ygeno.2006.12.014.

1062 101. Xiaohua Douglas Zhang. A new method with flexible and balanced control of false negatives
1063 and false positives for hit selection in rna interference high-throughput screening assays. *SLAS
1064 Discovery*, 12(5):645–655, August 2007. ISSN 24725552. doi: 10.1177/1087057107300645.

1065 102. Xiaohua Douglas Zhang. Strictly standardized mean difference, standardized mean difference and
1066 classical t-test for the comparison of two groups. *Statistics in Biopharmaceutical Research*, 2(2):
1067 292–299, May 2010. ISSN null. doi: 10.1198/sbr.2009.0074.

1068 103. Xiaohua Douglas Zhang. *Optimal High-Throughput Screening: Practical Experimental Design
1069 and Data Analysis for Genome-Scale RNAi Research*. Cambridge University Press, 1 edition,
1070 February 2011. ISBN 978-0-521-51771-3. doi: 10.1017/CBO9780511973888. URL <https://www.cambridge.org/core/product/identifier/9780511973888/type/book>.

1072 104. Xiaohua Douglas Zhang, Shane D. Marine, and Marc Ferrer. Error rates and powers in genome-
1073 scale rnai screens. *SLAS Discovery*, 14(3):230–238, March 2009. ISSN 2472-5552. doi: 10.1177/
1074 1087057109331475.

1075 105. Xiaohua Douglas Zhang, Raul Lacson, Ruojing Yang, Shane D. Marine, Alex McCampbell,
1076 Dawn M. Toolan, Tim R. Hare, Joleen Kajdas, Joel P. Berger, Daniel J. Holder, Joseph F.
1077 Heyse, and Marc Ferrer. The use of ssmd-based false discovery and false nondiscovery rates in

1078 genome-scale rnai screens. *SLAS Discovery*, 15(9):1123–1131, October 2010. ISSN 2472-5552. doi:
1079 10.1177/1087057110381919.

1080 106. Matthew P. Wand, John T. Ormerod, Simone A. Padoan, and Rudolf Frühwirth. Mean field
1081 variational bayes for elaborate distributions. *Bayesian Analysis*, 6(4):847–900, 2011. doi: 10.121
1082 4/11-BA631. URL <https://doi.org/10.1214/11-BA631>.

1083 107. Valentine Svensson. Droplet scrna-seq is not zero-inflated. *Nature Biotechnology*, 38(2):147–150,
1084 Feb 2020. ISSN 1546-1696. doi: 10.1038/s41587-019-0379-5.

1085 108. Valentine Svensson. Reply to: Umi or not umi, that is the question for scrna-seq zero-inflation.
1086 *Nature Biotechnology*, 39(2):160–160, Feb 2021. ISSN 1546-1696. doi: 10.1038/s41587-020-008
1087 11-5.

1088 109. F. Alexander Wolf, Philipp Angerer, and Fabian J. Theis. Scanpy: large-scale single-cell gene
1089 expression data analysis. *Genome Biology*, 19(1):15, Feb 2018. ISSN 1474-760X. doi: 10.1186/s1
1090 3059-017-1382-0.

1091 110. Lijia Yu, Yue Cao, Jean Y. H. Yang, and Pengyi Yang. Benchmarking clustering algorithms on
1092 estimating the number of cell types from single-cell rna-sequencing data. *Genome Biology*, 23(1):
1093 49, Feb 2022. ISSN 1474-760X. doi: 10.1186/s13059-022-02622-0.

1094 111. Nguyen Xuan Vinh, Julien Epps, and James Bailey. Information theoretic measures for clusterings
1095 comparison: is a correction for chance necessary? In *Proceedings of the 26th Annual International
1096 Conference on Machine Learning*, pages 1073–1080, 2009.

1097 112. Silke Wagner and Dorothea Wagner. Comparing clusterings - an overview, 2007. URL <https://publikationen.bibliothek.kit.edu/1000011477>.

1098 113. Zhuoqing Fang, Xinyuan Liu, and Gary Peltz. Gseapy: a comprehensive package for performing
1099 gene set enrichment analysis in python. *Bioinformatics*, 39(1):btac757, Jan 2023. ISSN 1367-4811.
1100 doi: 10.1093/bioinformatics/btac757.

1101 114. Suzi A Aleksander, James Balhoff, Seth Carbon, J Michael Cherry, Harold J Drabkin, Dustin
1102 Ebert, Marc Feuermann, Pascale Gaudet, Nomi L Harris, David P Hill, Raymond Lee, Huaiyu Mi,
1103 Sierra Moxon, Christopher J Mungall, Anushya Muruganugan, Tremayne Mushayahama, Paul W

1105 Sternberg, Paul D Thomas, Kimberly Van Auken, Jolene Ramsey, Deborah A Siegele, Rex L
1106 Chisholm, Petra Fey, Maria Cristina Aspromonte, Maria Victoria Nugnes, Federica Quaglia, Sil-
1107 vio Tosatto, Michelle Giglio, Suvarna Nadendla, Giulia Antonazzo, Helen Attrill, Gil dos Santos,
1108 Steven Marygold, Victor Strelets, Christopher J Tabone, Jim Thurmond, Pinglei Zhou, Saadul-
1109 lah H Ahmed, Praoparn Asanithong, Diana Luna Buitrago, Meltem N Erdol, Matthew C Gage,
1110 Mohamed Ali Kadhum, Kan Yan Chloe Li, Miao Long, Aleksandra Michalak, Angeline Pesala,
1111 Armalya Pritazahra, Shirin C C Saverimuttu, Renzhi Su, Kate E Thurlow, Ruth C Lovering, Colin
1112 Logie, Snezhana Oliferenko, Judith Blake, Karen Christie, Lori Corbani, Mary E Dolan, Harold J
1113 Drabkin, David P Hill, Li Ni, Dmitry Sitnikov, Cynthia Smith, Alayne Cuzick, James Seager,
1114 Laurel Cooper, Justin Elser, Pankaj Jaiswal, Parul Gupta, Pankaj Jaiswal, Sushma Naithani,
1115 Manuel Lera-Ramirez, Kim Rutherford, Valerie Wood, Jeffrey L De Pons, Melinda R Dwinell,
1116 G Thomas Hayman, Mary L Kaldunski, Anne E Kwitek, Stanley J F Laulederkind, Marek A
1117 Tutaj, Mahima Vedi, Shur-Jen Wang, Peter D'Eustachio, Lucila Aimo, Kristian Axelsen, Alan
1118 Bridge, Nevila Hyka-Nouspikel, Anne Morgat, Suzi A Aleksander, J Michael Cherry, Stacia R En-
1119 gel, Kalpana Karra, Stuart R Miyasato, Robert S Nash, Marek S Skrzypek, Shuai Weng, Edith D
1120 Wong, Erika Bakker, Tanya Z Berardini, Leonore Reiser, Andrea Auchincloss, Kristian Axelsen,
1121 Ghislaine Argoud-Puy, Marie-Claude Blatter, Emmanuel Boutet, Lionel Breuza, Alan Bridge,
1122 Cristina Casals-Casas, Elisabeth Coudert, Anne Streicher, Maria Livia Famiglietti, Marc Feuer-
1123 mann, Arnaud Gos, Nadine Gruaz-Gumowski, Chantal Hulo, Nevila Hyka-Nouspikel, Florence
1124 Jungo, Philippe Le Mercier, Damien Lieberherr, Patrick Masson, Anne Morgat, Ivo Pedruzzi,
1125 Lucille Pourcel, Sylvain Poux, Catherine Rivoire, Shyamala Sundaram, Alex Bateman, Emily
1126 Bowler-Barnett, Hema Bye-A-Jee, Paul Denny, Alexandre Ignatchenko, Rizwan Ishtiaq, Antonia
1127 Lock, Yvonne Lussi, Michele Magrane, Maria J Martin, Sandra Orchard, Pedro Raposo, Elena
1128 Speretta, Nidhi Tyagi, Kate Warner, Rossana Zaru, Alexander D Diehl, Raymond Lee, Juancar-
1129 los Chan, Stavros Diamantakis, Daniela Raciti, Magdalena Zarowiecki, Malcolm Fisher, Christina
1130 James-Zorn, Virgilio Ponferrada, Aaron Zorn, Sridhar Ramachandran, Leyla Ruzicka, and Monte
1131 Westerfield. The gene ontology knowledgebase in 2023. *Genetics*, 224(1):iyad031, March 2023.
1132 ISSN 0016-6731. doi: 10.1093/genetics/iyad031.

1133 115. The Tabula Sapiens Consortium*, Robert C. Jones, Jim Karkanas, Mark A. Krasnow, An-
1134 gela Oliveira Pisco, Stephen R. Quake, Julia Salzman, Nir Yosef, Bryan Bulthaup, Phillip Brown,

1135 William Harper, Marisa Hemenez, Ravikumar Ponnusamy, Ahmad Salehi, Bhavani A. Sana-
1136 gavarapu, Eileen Spallino, Ksenia A. Aaron, Waldo Concepcion, James M. Gardner, Burnett
1137 Kelly, Nikole Neidlinger, Zifa Wang, Sheela Crasta, Saroja Kolluru, Maurizio Morri, Serena Y.
1138 Tan, Kyle J. Travaglini, Chenling Xu, Marcela Alcántara-Hernández, Nicole Almanzar, Jane
1139 Antony, Benjamin Beyersdorf, Deviana Burhan, Kruti Calcuttawala, Matthew M. Carter, Charles
1140 K. F. Chan, Charles A. Chang, Stephen Chang, Alex Colville, Rebecca N. Culver, Ivana Cvijović,
1141 Gaetano D'Amato, Camille Ezran, Francisco X. Galdos, Astrid Gillich, William R. Goodyer, Yan
1142 Hang, Alyssa Hayashi, Sahar Houshdaran, Xianxi Huang, Juan C. Irwin, SoRi Jang, Julia Val-
1143 lve Juanico, Aaron M. Kershner, Soochi Kim, Bernhard Kiss, William Kong, Maya E. Kumar,
1144 Angera H. Kuo, Rebecca Leylek, Baoxiang Li, Gabriel B. Loeb, Wan-Jin Lu, Sruthi Mantri,
1145 Maxim Markovic, Patrick L. McAlpine, Antoine de Morree, Karim Mrouj, Shravani Mukherjee,
1146 Tyler Muser, Patrick Neuhöfer, Thi D. Nguyen, Kimberly Perez, Ragini Phansalkar, Nazan Pu-
1147 luca, Zhen Qi, Poorvi Rao, Hayley Raquer-McKay, Nicholas Schaum, Bronwyn Scott, Bobak
1148 Seddighzadeh, Joe Segal, Sushmita Sen, Shaheen Sikandar, Sean P. Spencer, Lea C. Steffes,
1149 Varun R. Subramaniam, Aditi Swarup, Michael Swift, Will Van Treuren, Emily Trimm, Stefan
1150 Veizades, Sivakamasundari Vijayakumar, Kim Chi Vo, Sevahn K. Vorperian, Wanxin Wang, Han-
1151 nah N. W. Weinstein, Juliane Winkler, Timothy T. H. Wu, Jamie Xie, Andrea R. Yung, Yue
1152 Zhang, Angela M. Detweiler, Honey Mekonen, Norma F. Neff, Rene V. Sit, Michelle Tan, Jia
1153 Yan, Gregory R. Bean, Vivek Charu, Erna Forgó, Brock A. Martin, Michael G. Ozawa, Oscar
1154 Silva, Angus Toland, Venkata N. P. Vemuri, Shaked Afik, Kyle Awayan, Olga Borisovna Botvin-
1155 nik, Ashley Byrne, Michelle Chen, Roozbeh Dehghannasiri, Adam Gayoso, Alejandro A. Grana-
1156 dos, Qiqing Li, Gita Mahmoudabadi, Aaron McGeever, Julia Eve Olivier, Madeline Park, Neha
1157 Ravikumar, Geoff Stanley, Weilun Tan, Alexander J. Tarashansky, Rohan Vanheusden, Peter
1158 Wang, Sheng Wang, Galen Xing, Les Dethlefsen, Po-Yi Ho, Shixuan Liu, Jonathan S. Maltz-
1159 man, Ross J. Metzger, Koki Sasagawa, Rahul Sinha, Hanbing Song, Bruce Wang, Steven E.
1160 Artandi, Philip A. Beachy, Michael F. Clarke, Linda C. Giudice, Franklin W. Huang, Ker-
1161 wyn Casey Huang, Juliana Idoyaga, Seung K. Kim, Christin S. Kuo, Patricia Nguyen, Thomas A.
1162 Rando, Kristy Red-Horse, Jeremy Reiter, David A. Relman, Justin L. Sonnenburg, Albert
1163 Wu, Sean M. Wu, and Tony Wyss-Coray. The tabula sapiens: A multiple-organ, single-cell
1164 transcriptomic atlas of humans. *Science*, May 2022. doi: 10.1126/science.abl4896. URL

1165 <https://www.science.org/doi/10.1126/science.abl4896>.

1166 116. Stephen R. Quake and The Tabula Sapiens Consortium. Tabula sapiens reveals transcription
1167 factor expression, senescence effects, and sex-specific features in cell types from 28 human organs
1168 and tissues. page 2024.12.03.626516, December 2024. doi: 10.1101/2024.12.03.626516. URL
1169 <https://www.biorxiv.org/content/10.1101/2024.12.03.626516v1>.

1170 117. Yuhao Hao, Stephanie Hao, Erica Andersen-Nissen, William M. Mauck, Shiwei Zheng, Andrew
1171 Butler, Maddie J. Lee, Aaron J. Wilk, Charlotte Darby, Michael Zager, Paul Hoffman, Mar-
1172 lon Stoeckius, Efthymia Papalexis, Eleni P. Mimitou, Jaison Jain, Avi Srivastava, Tim Stuart,
1173 Lamar M. Fleming, Bertrand Yeung, Angela J. Rogers, Juliana M. McElrath, Catherine A.
1174 Blish, Raphael Gottardo, Peter Smibert, and Rahul Satija. Integrated analysis of multimodal
1175 single-cell data. *Cell*, 184(13):3573–3587.e29, June 2021. ISSN 0092-8674, 1097-4172. doi:
1176 10.1016/j.cell.2021.04.048.

1177 118. M. Kanehisa and S. Goto. Kegg: kyoto encyclopedia of genes and genomes. *Nucleic Acids
1178 Research*, 28(1):27–30, January 2000. ISSN 0305-1048. doi: 10.1093/nar/28.1.27.

1179 119. Minoru Kanehisa. Toward understanding the origin and evolution of cellular organisms. *Protein
1180 Science: A Publication of the Protein Society*, 28(11):1947–1951, November 2019. ISSN 1469-
1181 896X. doi: 10.1002/pro.3715.

1182 120. Minoru Kanehisa, Miho Furumichi, Yoko Sato, Yuriko Matsuura, and Mari Ishiguro-Watanabe.
1183 Kegg: biological systems database as a model of the real world. *Nucleic Acids Research*, 53(D1):
1184 D672–D677, January 2025. ISSN 1362-4962. doi: 10.1093/nar/gkae909.

1185 121. Antonio Fabregat, Florian Korninger, Guilherme Viteri, Konstantinos Sidiropoulos, Pablo Marin-
1186 Garcia, Peipei Ping, Guanming Wu, Lincoln Stein, Peter D'Eustachio, and Henning Hermjakob.
1187 Reactome graph database: Efficient access to complex pathway data. *PLoS computational biology*,
1188 14(1):e1005968, January 2018. ISSN 1553-7358. doi: 10.1371/journal.pcbi.1005968.

1189 122. Antonio Fabregat, Konstantinos Sidiropoulos, Guilherme Viteri, Oscar Forner, Pablo Marin-
1190 Garcia, Vicente Arnau, Peter D'Eustachio, Lincoln Stein, and Henning Hermjakob. Reactome
1191 pathway analysis: a high-performance in-memory approach. *BMC bioinformatics*, 18(1):142,
1192 March 2017. ISSN 1471-2105. doi: 10.1186/s12859-017-1559-2.

1193 123. Antonio Fabregat, Konstantinos Sidiropoulos, Guilherme Viteri, Pablo Marin-Garcia, Peipei Ping,
1194 Lincoln Stein, Peter D'Eustachio, and Henning Hermjakob. Reactome diagram viewer: data struc-
1195 tures and strategies to boost performance. Bioinformatics (Oxford, England), 34(7):1208–1214,
1196 April 2018. ISSN 1367-4811. doi: 10.1093/bioinformatics/btx752.

1197 124. Johannes Griss, Guilherme Viteri, Konstantinos Sidiropoulos, Vy Nguyen, Antonio Fabregat,
1198 and Henning Hermjakob. Reactomegsa - efficient multi-omics comparative pathway analysis.
1199 Molecular & cellular proteomics: MCP, 19(12):2115–2125, December 2020. ISSN 1535-9484. doi:
1200 10.1074/mcp.TIR120.002155.

1201 125. Bijay Jassal, Lisa Matthews, Guilherme Viteri, Chuqiao Gong, Pascual Lorente, Antonio Fab-
1202 regat, Konstantinos Sidiropoulos, Justin Cook, Marc Gillespie, Robin Haw, Fred Loney, Bruce
1203 May, Marija Milacic, Karen Rothfels, Cristoffer Sevilla, Veronica Shamovsky, Solomon Shorser,
1204 Thawfeek Varusai, Joel Weiser, Guanming Wu, Lincoln Stein, Henning Hermjakob, and Peter
1205 D'Eustachio. The reactome pathway knowledgebase. Nucleic Acids Research, 48(D1):D498–D503,
1206 January 2020. ISSN 1362-4962. doi: 10.1093/nar/gkz1031.

1207 126. Marija Milacic, Deidre Beavers, Patrick Conley, Chuqiao Gong, Marc Gillespie, Johannes Griss,
1208 Robin Haw, Bijay Jassal, Lisa Matthews, Bruce May, Robert Petryszak, Eliot Ragueneau, Karen
1209 Rothfels, Cristoffer Sevilla, Veronica Shamovsky, Ralf Stephan, Krishna Tiwari, Thawfeek Varu-
1210 sasi, Joel Weiser, Adam Wright, Guanming Wu, Lincoln Stein, Henning Hermjakob, and Pe-
1211 ter D'Eustachio. The reactome pathway knowledgebase 2024. Nucleic Acids Research, 52(D1):
1212 D672–D678, January 2024. ISSN 0305-1048. doi: 10.1093/nar/gkad1025.

1213 127. Konstantinos Sidiropoulos, Guilherme Viteri, Cristoffer Sevilla, Steve Jupe, Marissa Webber,
1214 Marija Orlic-Milacic, Bijay Jassal, Bruce May, Veronica Shamovsky, Corina Duenas, Karen
1215 Rothfels, Lisa Matthews, Heeyeon Song, Lincoln Stein, Robin Haw, Peter D'Eustachio, Peipei
1216 Ping, Henning Hermjakob, and Antonio Fabregat. Reactome enhanced pathway visualization.
1217 Bioinformatics (Oxford, England), 33(21):3461–3467, November 2017. ISSN 1367-4811. doi:
1218 10.1093/bioinformatics/btx441.

1219 128. Guanming Wu and Robin Haw. Functional interaction network construction and analysis for

¹²²⁰ disease discovery. Methods in Molecular Biology (Clifton, N.J.), 1558:235–253, 2017. ISSN 1940-
¹²²¹ 6029. doi: 10.1007/978-1-4939-6783-4_11.